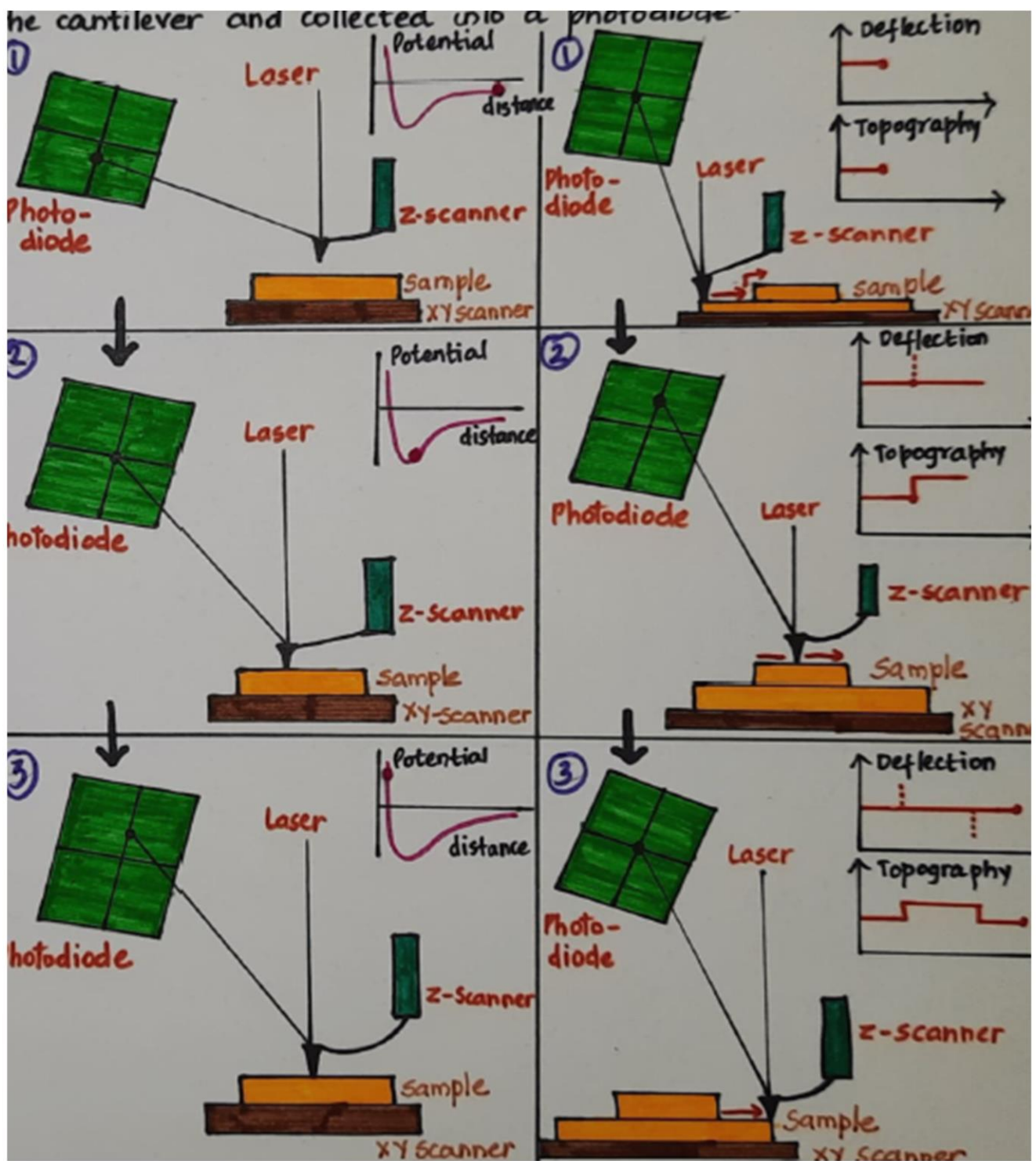


A Glimpse Of The Atomic World: Atomic Force Microscopy (AFM)



ATOMIC FORCE MICROSCOPY (AFM)

A literature review submitted in partial fulfilment of the requirements for the degree of

Master of Science in Chemistry.

BY

Neha Yogesh Raikar



School of chemical sciences

Goa university, Taleigao, Panaji-Goa 2021-2022

DECLARATION

I declare that the literature review titled “A glimpse of the Atomic World: Atomic Force Microscopy” has been carried out by me in the Chemistry Department, School of Chemical Sciences, Goa University. The Information derived from the literature has been duly acknowledged in the text and a list of references is provided.

AKNOWLEDGMENT

The literature review titled: "A glimpse of the atomic world: Atomic Force Microscopy" has been successfully completed under the guidance of Dr. Vivekanand Vaman Gobre during the year 2021-2022 in the partial fulfilment of the requirements for the degree of Master of Science in Chemistry.

I had a good learning experience learning the importance and future prospects of undertaking a literature survey which was possible due to the timely guidance of Dr. Vivekanand Vaman Gobre and our respected Dean Dr. Vidhyadatta Verenkar. I also thank the entire library faculty for helping me out for searching relevant books with respect to my topic.

Last but not the least I thank my parents, friends and other people who are directly or indirectly in the successful completion of my Literature survey.

Contents

Section 1

Introduction.....

Section 2: Working principle of AFM

2.1 Components of AFM.....

2.2. Piezocrystals.....

2.3. AFM probes.....

2.4. Beam Deflection.....

2.5. Forces versus the distance.....

2.6. Modes of operation in AFM.....

2.7. Advantages and disadvantages of AFM modes.....

Section 3: Literature review of applications of AFM

1. Biological materials.

2. Surface analysis of materials.

3. Nanomaterials

Introduction

In 1986, a Nobel prize in Physics was shared by Gerg Binning and Henrich Rocher¹ for inventing the scanning tunneling microscope and discovering that it can image individual surface atoms with unprecedented resolution. The success of the scanning tunneling microscope has given birth to the invention of a host of other scanning probe microscopes which rely on mechanically scanning a sharp tip over a sample surface. AFM waved itself with a revolution. It made it possible to capture images with high resolution with relatively cheap and a simple instrument. AFM is an instrument that traces the surface topography of the sample with a sharp probe while monitoring the interaction forces working between the probe and sample surface. Thus, it provides three-dimensional surface images of the sample with high resolution and accuracy. It helps us to get images with the arrangement of individual atoms in a sample or to see the structure of an individual molecule. Although the most fundamental advancement for scientific research credit was given to STM, it had its limitations, because it worked only with chemically conductive samples². Despite of these limitations STM remains a very useful technique and is used in particular in physics and material science to characterize the atomic structure of metals and semiconductors and thus for the fundamental studies of electronic effects at metal surfaces³. In AFM, cryogenic temperatures by scanning in ultra-high vacuum, the hopping of individual atoms from a surface has been measured. Even very small images of 5nm in size and very large images of 100 micro-meters can be measured⁴.

The greatest advantage of AFM is that almost any sample can be imaged, be it be a ceramic material (hard sample) or a dispersion of metallic nanoparticles or flexible polymers (soft sample), human cells or individual DNA molecules⁵.

AFM if compared with other microscopes is rather different because it does not form an image by focussing light or electrons onto a surface like an optical or electron on microscope. There is no concept of illumination of the sample in it's operation. AFM with it's shape probe, literally feels the sample surface, and builds up a map of the height of the sample's surface. This makes it very simple to quickly measure the height, length, width or volume of any feature in the image².

Soon after AFM was invented, a much more reproducible cantilever manufactured by silicon lithography replaced the gold leaf/diamond combination which enables the production of more than 400 cantilevers on a single 7-inch wafer⁶. AFM has come to be used in all fields of science such as chemistry, biology, physics, material science, nanotechnology, astronomy, medicine and more.

However, AFM has been modified to measure huge number of different properties and perform lots of additional (non- imaging experiments) and combined with techniques having greater flexibility in terms of types of samples scanned⁴. This report will fully focus on AFM, with it's detailed study of it's applications in various fields and it's future prospects.

Working principle of afm

The AFM working principle is the measurement of the interactive force between a tip and the sample surface using special probes made by an elastic cantilever with a sharp tip on the end. The force applied on the tip by the surface, results in bending of the cantilever. This helps to evaluate the tip-surface interactive force. The interactive forces measured by AFM can be quantitatively explained by considering for example the van der Waals forces which is the potential energy of two atoms located at a distance r from each other, is approximated by the exponential function-Lennard-Jones potential:

$$ULD(r) = U_0 \left\{ -2 \left(\frac{r_0}{r} \right)^6 + \left(\frac{r_0}{r} \right)^{12} \right\}$$

The first term of the sum describes the long-distance attraction caused by a dipole-dipole interaction and the second term takes into account the range repulsion due to the Pauli exclusion principle.

Components of afm

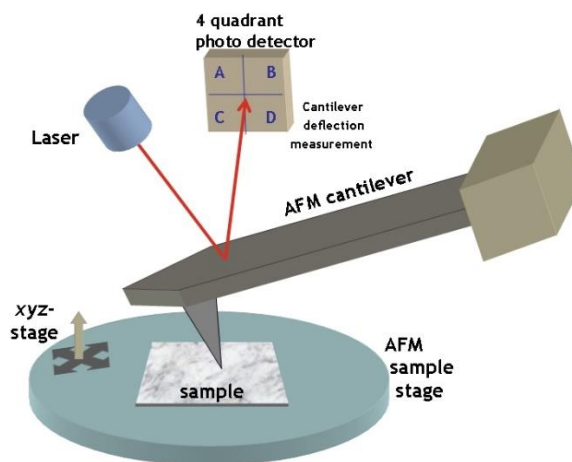


Fig.A: Schematic picture of AFM components.

Piezocrystals

Piezocrystals are ceramic materials that expand or contract in the presence of voltage gradient and conversely, they develop an electrical potential in response to mechanical pressure. In this way, movements in x, y and z direction are possible.

Probes in afm

The probe represents a micromachined cantilever with a sharp tip at one end, which is brought into interaction with the sample surface. Each probe has different specifications and shape. V-shaped cantilevers are the most popular (but also there are rectangular), providing low mechanical resistance to vertical deflection, and high resistance to lateral torsion. Cantilevers typically range from 100 to 200 μm in length (l), 10 to 40 μm in width (w), and 0.3 to 2 μm in thickness (t). Integrated cantilevers are usually made from silicon (Si) or silicon nitride (Si_3N_4). They are characterized by their force constant and resonant frequency, which have to be chosen according to the sample to be studied. Additionally, an optical detection system and electronics for the management of scanning procedures and data acquisition are necessary.

Beam deflection detection

To detect the displacement of the cantilever, a laser is reflected off the back of the cantilever and collected in a photodiode. The diode is divided into four parts, as seen in Figure A. When the laser is displaced vertically along the positions top (B-A) and bottom (D-C), there exists a bending due to topography, while if this movement is horizontal left (B-D) and right (A-C), it produces a torsion due to “friction” (lateral force).

Forces versus the distance

A force sensor in an AFM can only work if the probe interacts with the force field associated with a surface. The dependence of the van der Waals force upon the distance between the tip and the sample is shown in Figure B. In the contact regime, the cantilever is held less than a few angstroms from the sample surface, and the interatomic force between the cantilever and the sample is repulsive. In the non-contact regime, the cantilever is held on the order of tens to hundreds of angstroms from the sample surface, and the interatomic force between the cantilever and sample is attractive (largely a result of the long-range Van der Waals interactions).

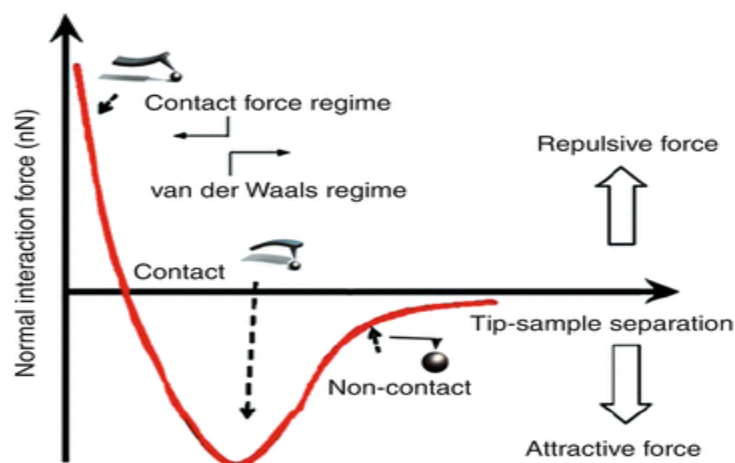


Fig.B: Potential energy diagram of a probe and sample.

Modes of operation in afm

A) **Contact mode**: The tip makes soft physical contact with the surface of the sample. The tip either scans at a constant small height above the surface or under conditions of a constant force. In constant height mode the height of the tip is fixed whereas in constant force mode the deflection of the cantilever is fixed and the motion of the scanner in Z- direction is recorded.

B) **Non-contact mode:** The probe operates in the attractive force region and the tip-sample interaction is minimized. This allows scanning without influencing the shapes of the sample by the tip sample forces.

C) **Tapping mode (intermittent mode):** The cantilever oscillates close to its resonance frequency. An electronic feedback loop ensures that the oscillation amplitude remains constant, such that a constant tip-sample interaction is maintained during scanning.

Feedback mechanism

The relative distance between the tip and the sample must be in a particular range during the whole sweep ensures the accuracy of the measurement. The reason for this is this separation is high, the strength of the force becomes so weak that the noise dominates over the signal. On the other hand if the distance between the tip and the sample is too small, a large force is exerted by the tip on the sample surface which may cause damage to the instrument or the sample itself. To solve this issue, a feedback loop control is introduced in the AFM device.

Advantages and disadvantages of atomic force microscopy

Advantages:

The contact mode in AFM has high scanning speeds, high atomic resolution and makes it easier to scan rough samples with extreme changes in vertical topography. The Non-contact mode in AFM exerts a low force on the sample surface and no damage is caused to the soft samples. Finally the tapping mode (intermittent mode) provides higher lateral resolution (1nm to 5nm), exerts lower forces and less damage to soft samples in air and has almost no lateral forces.

Disadvantages:

In the contact mode of AFM the lateral forces can distort the image produced. The capillary forces form a fluid layer which can cause large forces normal to the tip-sample interaction. Combination of these forces reduces spatial resolution and can cause damage to soft samples. The non-contact mode in AFM is applicable in extremely hydrophobic samples with minimal fluid layer. Lower lateral forces operating in the non-contact mode of AFM is lowered and is limited by the tip-sample interaction. Scanning speeds are slower in non-contact mode (because the contact between the tip and the sample is minimized) as well as in tapping mode of AFM.

1. Imaging and manipulation of biological structures with afm

AFM is also a unique technique to understand the assemblies of biomolecules i.e supramolecular assemblies and the fundamental importance to elucidate their structure and provide information at the single molecular level¹³. This kind of a nanomanipulation experiment was first performed on genetic material¹⁴. The DNA in the eukaryotic nucleus is packaged with proteins to form chromatin which further condenses to form chromosomes (visible during metaphase as distinct morphological entities)¹³.

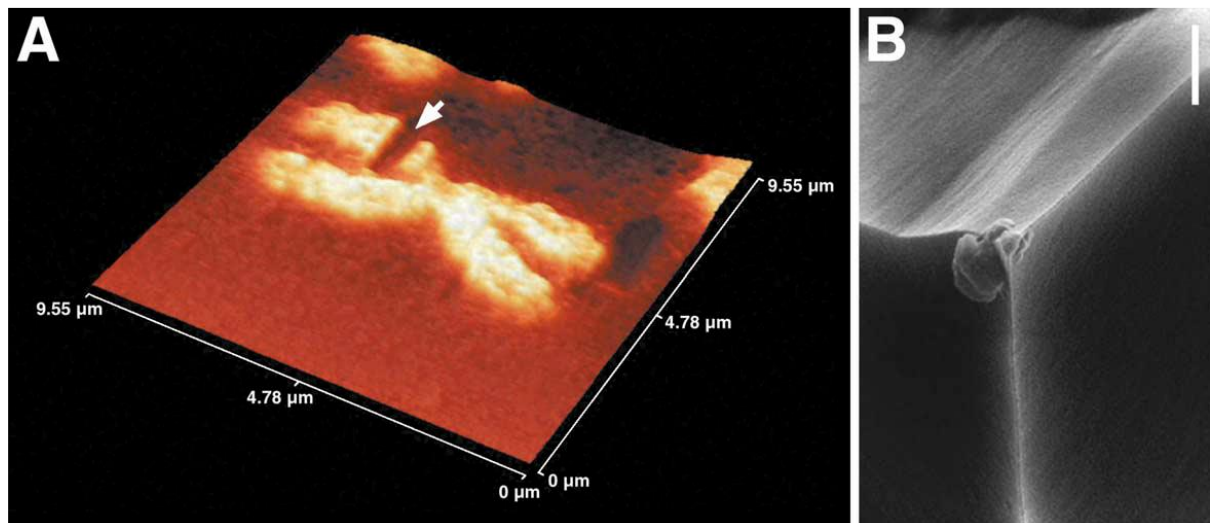


Fig.4: (A) AFM topograph of human chromosome 2 recorded after dissection. The DNA dissection is marked. (B) Scanning electron microscopy image of the AFM probe after DNA extraction.

Plant, insect¹⁵, human chromosome topographs¹³ with nanometer lateral resolution and sub-nanometer vertical resolution have been imaged by the AFM. Recent studies labelling techniques have discovered an application in combination light and atomic force microscopy in parallel to examine cells under physiological conditions, to determine the position of the structures which are labelled with fluorescent markers¹⁶.

Native surface structures of membrane proteins which are incorporated into a lipid bilayer has been examined using atomic force microscopy. However the membrane proteins which are sandwiched could cause a problem because the extracellular surface must be left uncovered in order for the AFM probe to interact with them¹⁷.

Membrane proteins inhibit their function through specific folding of their polypeptide chain and through unique interactions with the lipid bilayer and surrounding proteins. These interactions are responsible for their overall stability and resistance. So, AFM along with single molecule force spectroscopy have been able to monitor the forces that anchor membrane proteins in the lipid bilayer ¹³.

2. Application of afm in the study of microbiologically influenced corrosion

The use of AFM has also been widely done for high resolution topographical imaging of bacteria, biofilm and corroded steel surfaces and in the quantification of corrosion at the desired position²⁰. A biofilm is formed when microorganisms attach themselves to solid surfaces, colonize, proliferate. The biofilm, consists of heterogeneous bacteria along with extracellular polymeric substance (EPS), creates gradients of pH, dissolved oxygen, and chloride, leading to the localized corrosion of materials. It is experimentally observed that 20% of corrosion is due to the MIC. Bacteria colonization on a copper surface was observed using AFM²¹. Another study reported a sulphate-reducing bacteria (SRB) biofilm corrosion and the sub- micrometer features of marine SRB cells on mica were visualised²².

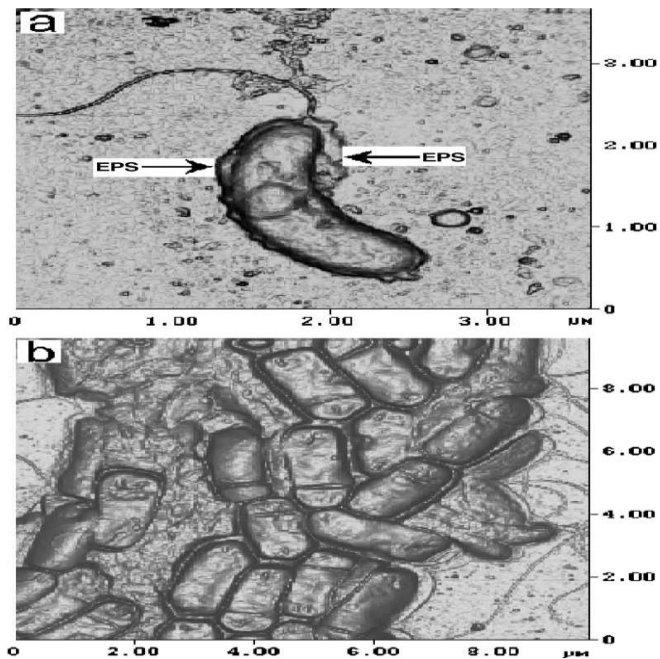


Fig.6 : displays a typical AFM images which have superior resolution and definition in the vertical dimension of an isolated SRB cell attached on the mica surface after immersing it for one hour in seawater. The image clearly shows the shape and flagella of the bacteria and when these cells multiplied in the sea water which is a nutrient rich medium they grew and aggregated to form the clusters seen in fig 5b (image taken after 8 h of immersion).

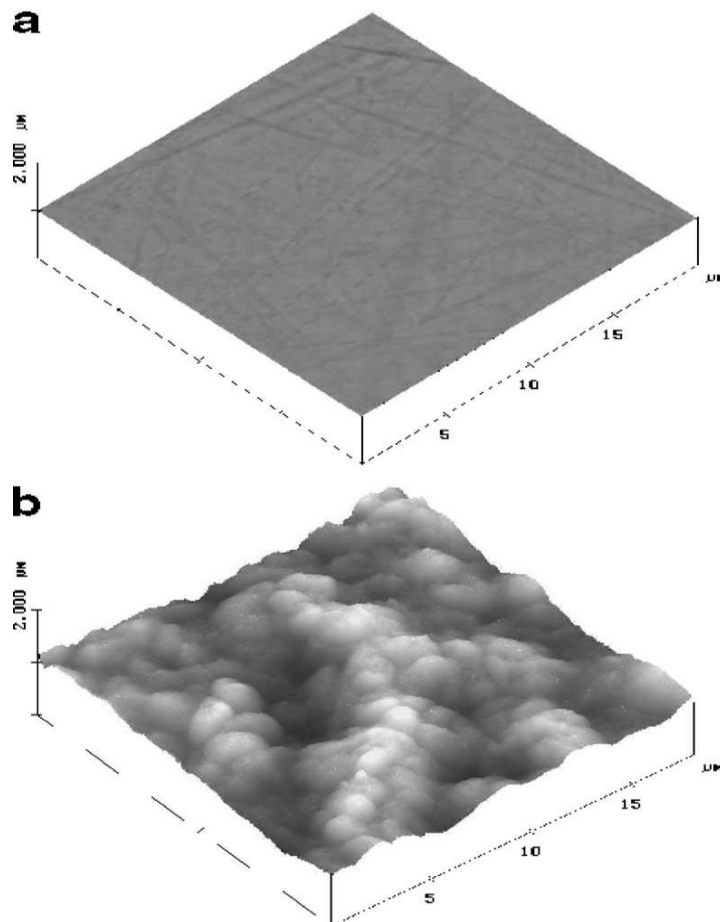


Fig.7: shows an AFM image of a pre-exposed mild steel surface and a steel surface which is 20 day old biofilm.

3. Atomic force microscopy for studying dna (deoxyribo nucleic acid) and chromosomes

Previous studies have been reported that DNA molecules do not bind strongly to mica and are usually moved or swept away by the scanning tip, due to the fact that freshly cleaved mica and DNA are both negatively charged. Therefore, the mica surface was often treated with Mg^{++} and a variety of other divalent and trivalent cations for the AFM observation of DNA. However, the following experiments²³ show that DNA molecules, when dissolved in distilled water, consistently bind to freshly cleaved mica at rates sufficient for imaging with the non-contact mode AFM.

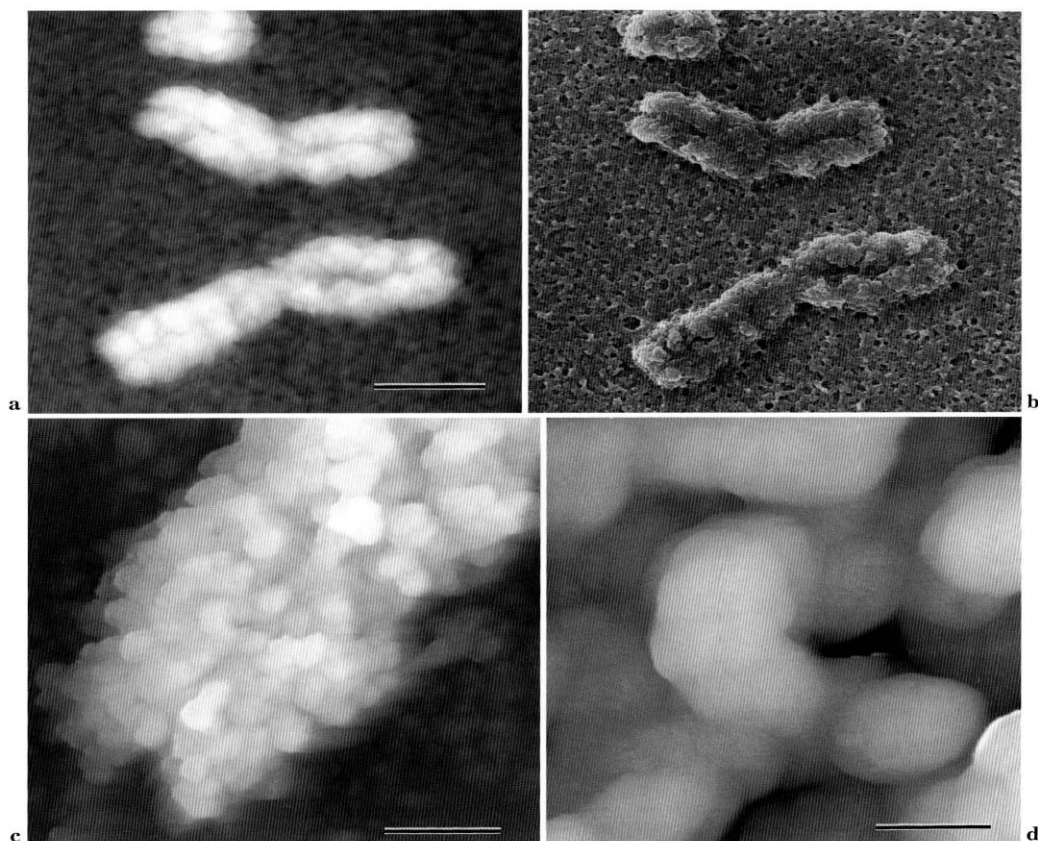


Fig. 8. AFM (a, c, d) and SEM (b) images of human metaphase chromosomes. AFM data are obtained in a non-contact mode in air.

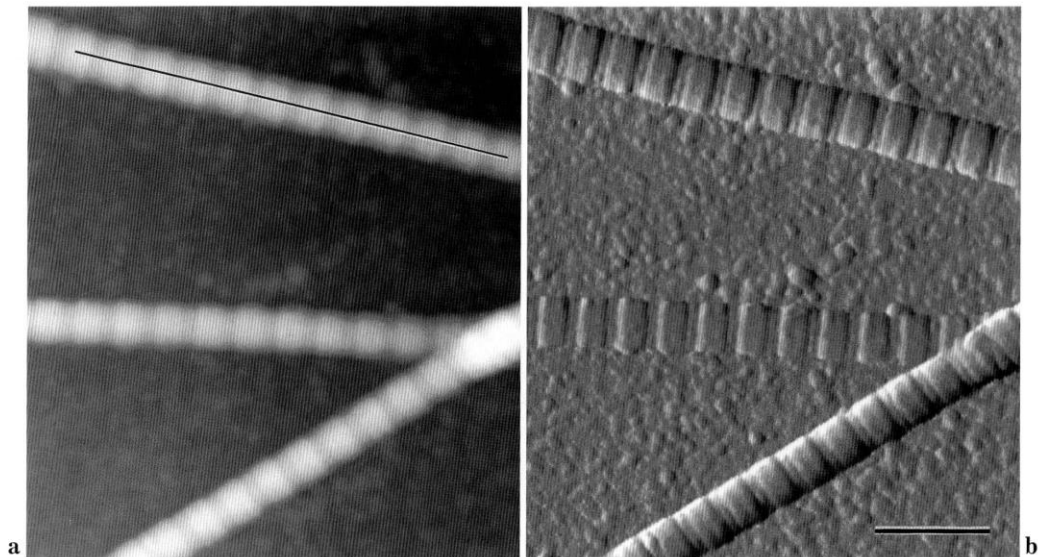


Fig.9A: AFM images of collagen fibrils measured in a non-contact mode in air. The data were obtained simultaneously as the height image (a) and variable deflection image (b). In the height image, the z-scale from black (low) to white (high) corresponds to 61.5 nm. Bar is 200 nm.

Chromosomes are suitable samples for the AFM study as well Human metaphase chromosomes were prepared by the standard method used for light microscopy. Peripheral blood cultures were treated with a hypotonic solution of potassium chloride and fixed with a mixture of methanol and acetic acid (3: 1 ratio). Chromosome spreads were made by dropping the fixed cell suspension onto 0.1% poly-L-lysine coated glass slides, followed by air-drying. Several minutes later after drying, the slides were rinsed in phosphate buffer and treated with 1 % osmium tetroxide for about 10 minutes. Some specimens were rinsed in 0.025% trypsin in 0.85% saline for 30 sec and fixed in phosphate-buffered glutaraldehyde prior to osmication. All specimens were dehydrated in absolute ethanol and critical point dried in liquid CO₂. AFM imaging was carried out in air in a non-contact mode.

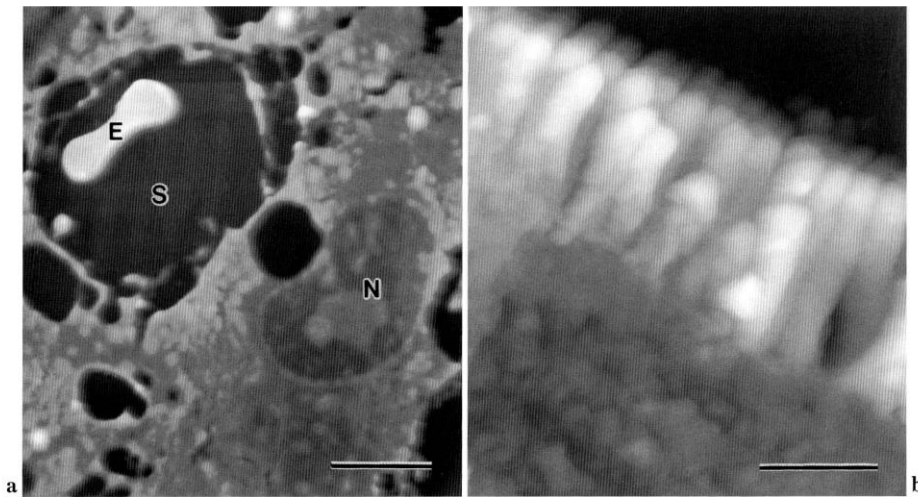


Fig.9B: AFM images of the embedment-free sections prepared according to the polyethylene glycol embedding and subsequent de-embedding method. The data were obtained in a non-contact mode in air and displayed as gradation images of the height mode.

4. Application of atomic force microscopy in mineral flotation

AFM has been employed to image mica, galena, molybdenite and phyllosilicate which are pure mineral surfaces. To prepare clean, atomically flat surfaces all these mineral surfaces can be easily cleaved. For example, Gupta et al. ⁷, AFM was used to image the crystal lattice of silica and alumina faces of phyllosilicate (kaolinite). To deposit Kaolinite negatively charged glass or mica and positively charged alumina were used as the substrates. Due to the electrostatic double-layer attraction, the positively charged alumina face of kaolinite particles attached to the glass or mica surface, thus exposing the silica faces. In contrast, the alumina face of kaolinite particles were exposed, when alumina was used as a substrate. It was found that tetrahedral oxygen atoms on the silica face formed a closed hexagonal ring-like network with a vacancy in the centre. The hexagonal lattice ring of hydroxyls surrounded a hydroxyl was observed on the alumina face and the atomic spacing between neighbouring hydroxyls was determined as $0.36 \pm 0.04 \text{ nm}^8$.

The basal (001) planes of various types of phyllosilicates, namely gibbsite, kaolinite, Illite, and Na-montmorillonite (Fig 1), in water was observed under AM-AFM. All pictures show the trademark hexagonal construction with a periodicity ≈ 0.5 nm that emerges from the semi hexagonal plan of silica-tetrahedra and alumina-octahedra, the classical building units of all mud materials⁹. In sulfide mineral buoyancy the oxidation state is vital. The floatability or buoyancy of sulfide minerals is straight connected with the level of its surface oxidation. For instance, new galena is hydrophilic. It was observed that slight surface oxidation expanded the hydrophobicity and floatability of galena because of the development of sulfur rich layers.

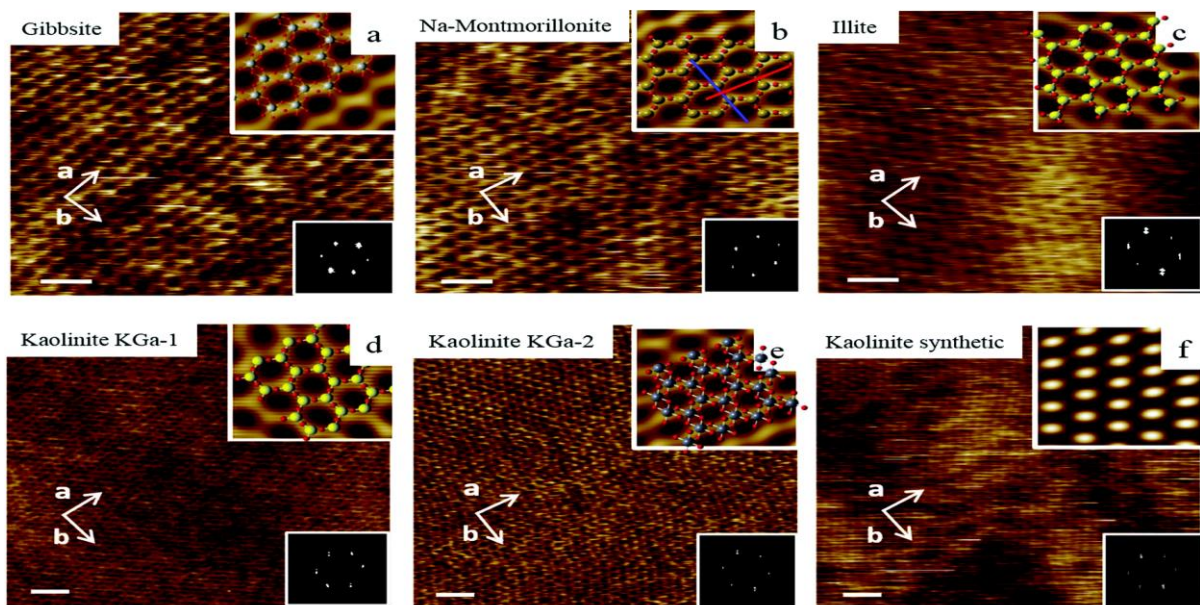


Fig 1 : Atomic resolution AFM images of clays basal plane: (a) gibbsite, (b) Na-montmorillonite, (c) illite and (d–f) kaolinite clay particles obtained with super sharp tip at room temperature equilibrated in ultrapure water.

Hence, collectorless buoyancy of sulfide minerals becomes conceivable by changing the surface oxidation^{9,10}. Xie et al. studied¹¹ the impact of applied electrochemical potential, concerning the Ag/AgCl/3.4 M KCl reference terminal, on the galena surface morphology at pH 5.6. It was observed that surface harshness expanded fundamentally when the potential surpassed +300 mV (Fig.2) This was because of the agglomeration of electrochemical

oxidation items on the galena surface. Hampton et al concentrated on the impact of applied potential on electrochemical oxidation of the galena surface at pH 4.5 Sulfur spaces were noticed and surface harshness expanded when the electrochemical potential expanded to +258 mV.

Hampton et al. ¹¹, reasoned that the electrochemical oxidation of galena is a two-venture process: First, sulfur is delivered into the arrangement and then the sulfur stores on ideal locales; the sulfur spaces are dispersed heterogeneously⁹ (Fig.3) while in Xie's report, the sulfur areas were all the more homogeneously appropriated.

The justification for this disparity might be because of the expanded surface harshness of galena in Hampton's investigation. Surface heterogeneity prompted a heterogeneous dispersion of oxidation items.

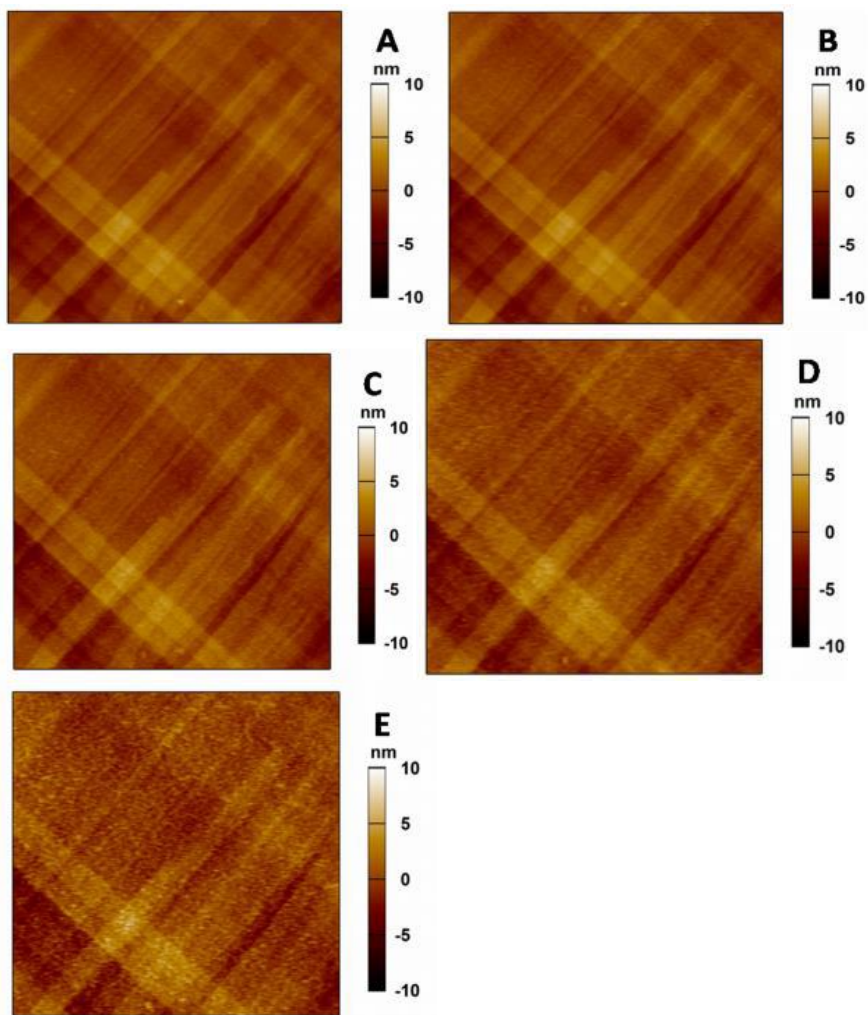
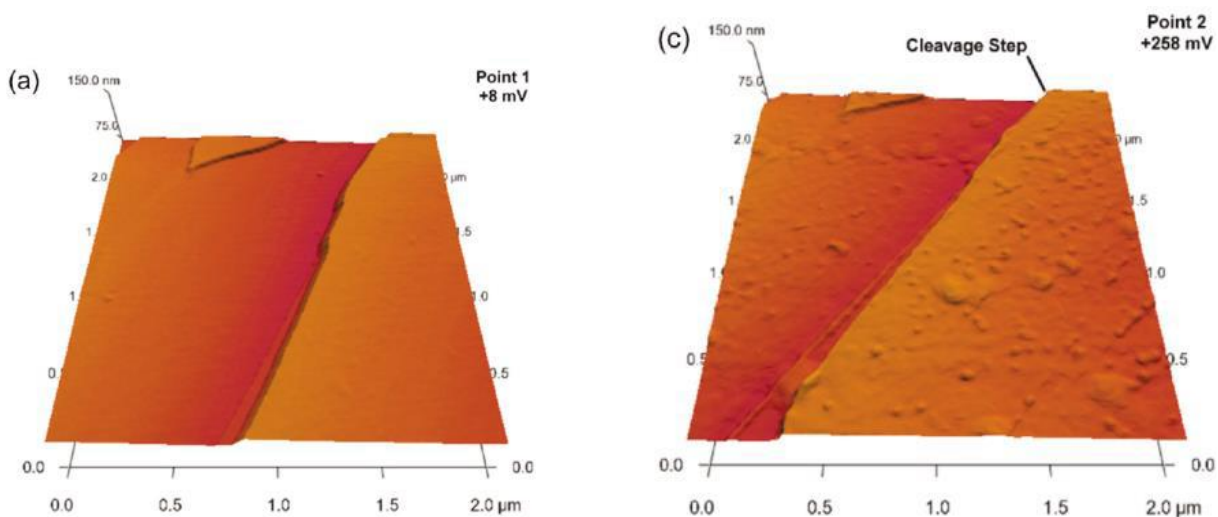


Fig. 2: Surface topographies of galena surfaces under different applied potentials in 0.5 M NaCl: (A) -700 mV, (B) -300 mV, (C) 0 mV, (D) 300 mV, and (E) 450 mV.



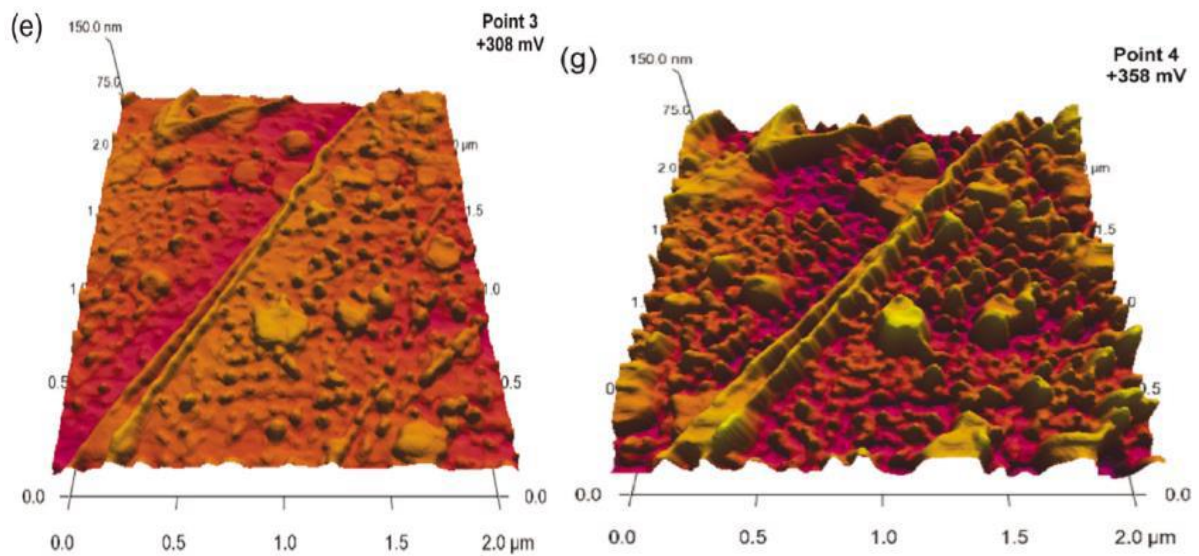


Fig.3: Surface topographies of galena surfaces under different applied potentials: A, +8 mV; B, +258 mV; C, +308 mV; D, +358 mV.

For non-unadulterated minerals which don't have a cleavage face, pre-treatment, for example, cautious cleaning is expected to bring down the surface unpleasantness with the goal that it tends to be imaged by AFM. Bruening and Cohen¹² applied AFM to recognize the surface harshness varieties when coal oxidation.

5. Study of natural and model soil

Particles with afm

The structure and surface chemistry of soil particles has extensive impact on many bulk scale properties and processes of soil systems and consequently the environments that they support. There are a number of physiochemical mechanisms that operate at the nanoscale which affect the soil's capability to maintain native vegetation and crops; this includes soil hydrophobicity and the soil's capacity to hold water and nutrients. The present study used atomic force microscopy in a novel approach to provide unique insight into the nanoscale properties of natural soil particles that control the physiochemical interaction of material within the soil column. There have been few atomic force microscopy studies of soil, perhaps a reflection of the heterogeneous nature of the system. The present study adopted an imaging and force measurement research strategy that accounted for the heterogeneity and used model systems to aid interpretation²⁵. The surface roughness²⁶ of natural soil particles increased with depth in the soil column a consequence of the attachment of organic material within the crevices of the soil particles.

7. The ecomechanics of gecko adhesion: natural surface topography, evolution, and biomimetics

The investigation of gecko attachment is fundamentally interdisciplinary due to the progressive nature of the glue framework and the intricacy of co-operations between the creatures and their living spaces. In nature, geckos continue on a wide scope of surfaces counting delicate sand hills, trees, and shakes, yet a significant part of the exploration over the past twenty years has zeroed in on their glue execution on counterfeit surfaces.

Investigating the intricate connections among geckos and their regular territories will uncover parts of the cement framework that can be applied to biomimetic research, for example, the elements that work with development on messy and unpleasant surfaces with changing microtopography. Moreover, differentiating set-ups of limitations and geologies are found on rocks and plants, probable driving contrasts in headway also, morphology. Our overall objectives are to expose a few parts of environment that are significant for gecko-natural surroundings co-operations, and to propose a system for how they can rouse material researchers and useful scientists. Additionally present research provides new information on surface harshness and geography of an assortment of surfaces, and glue execution of *Phelsuma geckos* on varying surfaces³². Despite the fact that surface harshness is of central significance to attachment between gecko toe cushions and the surfaces they use³³, we really have barely any insight into the reasonable limitations that limit gecko cement execution on one or the other normal or engineered substrates.

The deficiency of studies measuring substrate use by free-going geckos, and the focal point of most research center studies on cement execution on abnormally smooth substrates (e.g., glass) is as it were a contributor to the issue. A more crucial test includes the specialized and hypothetical challenges associated with describing the rough of surfaces in general³⁴. Adhesion to rough surfaces emerges from fascination between iotas of the gecko skin and molecules of the reached surface, conceivable as it were with versatile disfigurement of the materials which allows not as much as nanometer detachment. However, surface roughness can stretch out over

numerous length scales that are pertinent to connecting at the smallest scales.

The origin of gecko adhesion is challenging to address as most pad-bearing geckos have a fully-developed system that develops extremely high shear adhesive strength. However, there are cases where adhesion is evident with only the rudiments of toe pads being present. Such cases provide a window into the origin of adhesion and the associated ecological context. *Gonatodes* is a prime example of a genus in which adhesion is associated with incipient toe pads. Most species of this genus are incapable of generating measurable adhesive force³⁵, but *G. humeralis* is unique in having branched setae and adhesive capabilities^{35 36}, and can ascend a vertical sheet of smooth acrylic, an impressive feat for a gecko without well developed toepads³⁵. What selective pressures may favor the transformation of spinules (tiny hairlike growths) into adhesive setae? One scenario involves the opening up of new areas of a habitat (smoother and higher), allowing geckos to avoid competition by partitioning resources.

Having the ability to increase friction would potentially enable a gecko to remain stationary on a smooth leaf surface when sleeping.

In Trinidad, *G. humeralis* frequently occupies vertical smooth bamboo shoots, a challenging substrate that is not occupied by other lizards³⁵. Individuals of this species move very little (2.3% of observation time) and perch with their head down the majority (68%) of the time³⁷. This posture is compatible with a directional adhesive and with a reduction in energy expenditure. There is strong evidence for pad-bearing lizards dividing resources in their habitat^{38,39}, and these are often accompanied by morphological, performance, or behavioral shifts.

Many geckos will perch on leaves, often to sleep⁴⁰. However, plant surfaces are used by some gecko groups routinely during locomotion. This can include tree trunks, leaves, and the surfaces of fruits, or flowers. Thus, the

surfaces of plants have likely been critical in driving the evolution of, and molding the function of, the gecko adhesive apparatus. Indeed, some geckos (especially those of the genus *Phelsuma*) exhibit mutualistic relationships with flowering species by consuming their nectar and acting as pollinators^{41,42,43}. Therefore, there is potential for coevolution between geckos and plants in the context of feeding and reproduction, but whether this translates into the evolution of plant surfaces that facilitate gecko adhesion is currently unknown. Three species of *Phelsuma* were examined to cling to smooth acrylic, a leaf of the succulent *Sansevieria* ($Sq = 1.67 \mu\text{m}$) and, to mimic a rocky surface, 600-grit sandpaper ($Sq = 4.85 \mu\text{m}$). The methods followed those of³⁵. Relative to acrylic, all three species exhibited a large drop in performance (at least 30%) on the *Sansevieria*, and another drop on the sandpaper. From this limited sample it is evident that even a "smooth" leaf has asperities that can result in a drop in adhesive ability. Therefore, categorizing surfaces as "smooth" without thorough investigation is problematic. Naylor and Higham (2019) assessed how the turnip-tailed gecko (*Thecadactylus rapicauda*) adheres to both natural plant surfaces and a series of artificial surfaces.

For plants, only smooth and "hairy" leaves were compared, with the latter being covered by fairly long (up to 1mm) trichomes. Indeed, frictional adhesive performance was significantly lower on the rough "hairy" leaf ($Sq = 94.1 \mu\text{m}$) compared to the smooth leaf ($Sq = 6.4 \mu\text{m}$). Therefore, for those geckos that perch on leaf surfaces for extended periods of time, or for those small geckos that traverse leaves on a regular basis, leaf microstructure could have a profound influence on performance and survival. This warrants a rigorous investigation of the microtopography of leaves exploited by geckos in nature. For smaller geckos on large leaves, different parts of a leaf could be preferentially used during locomotion³².

For example, some *Phelsuma* species (e.g. *P. sundbergi*) occupying large trees (e.g. *Lodoicea maldivica*) preferentially move on petioles, the trunk, or inflorescences ³⁵.

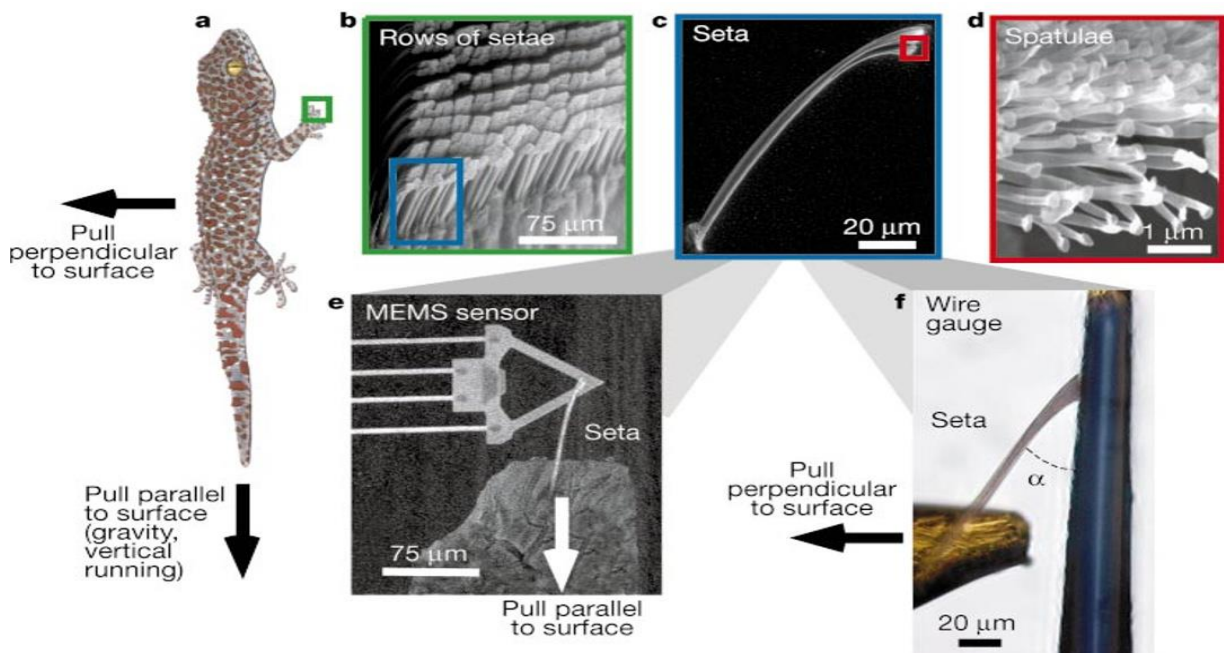


Fig.12: Gecko setae and apparatus for force measurement. a, Tokay gecko (Gekko gecko) with toe outlined. b-d, SEMs of rows of setae from a toe (b), a single seta (c) and, the nest terminal branches of a seta, called spatulae (d). e, Single seta attached to a micro-electromechanical system (MEMS) cantilever⁷ capable of measuring force production during attachment parallel and perpendicular to the surface. f, Single seta attached to an aluminum bonding wire capable of measuring force production during detachment perpendicular to the surface. Angle between setal stalk and wire represented by α .

8. Surface characterization of butterfly wings

Butterflies are notable to have water repellent wings that assist them to make due in conditions with steady precipitation. The hydrophobicity instruments of butterfly wings can be credited to the sub-micron scale highlights. Wu et al⁴⁴ directed morphological examinations on the wing sizes of six butterfly species living in upper east of China. They moreover introduced 3D models considering wing structures acquired from optical microscopy, filtering electron microscopy and transmission electron microscopy. Chen et al⁴⁵ portrayed wettability and self-cleaning impact of butterfly wing surfaces utilizing confocal light microscopy. The residue on

a superficial level can effectively be cleaned by moving round water beads when the slanting point is bigger than 3° . It was finished up from their concentrate on that nanostructure assumes a vital part in the self-cleaning capacity. Burton and Bhushan⁴⁵ portrayed the bond and contact properties of hydrophobic leaf surfaces. Optical profiler and nuclear power microscopy were utilized in the portrayal to make the estimations on leaves with and without wax on a superficial level. It was shown that both miniature knock and wax assume a similarly significant part in the hydrophobic nature as well as the grip and rubbing of leaf.

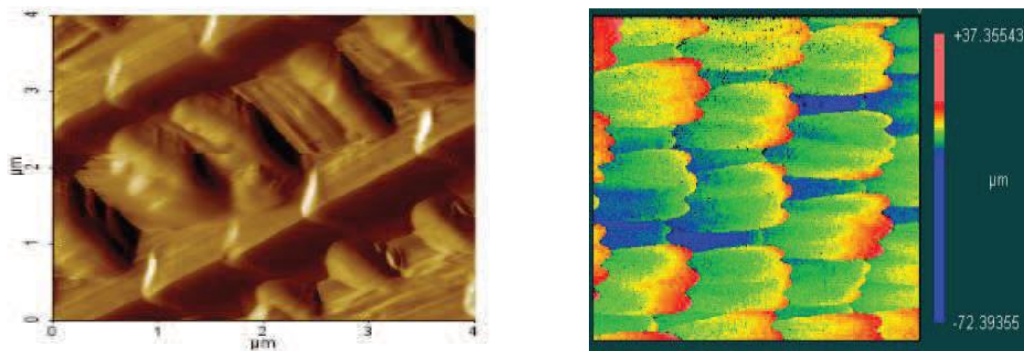


Fig.13: Images showing the nano and micro structures of the ‘*Phoebis Philea*’ (a) AFM image of 4 x 4 μ m² (b)optical profilometer image of 350X260 μ m²

The butterfly *Phoebis Philea*'s upper wing surface was scanned with different scan sizes using non-contact mode AFM. The raw data generated from the scanned image was used in calculating the roughness factor, which is defined as the ratio of true surface area to projected area. The roughness factors for different scan sizes are plotted. For smaller scan areas, the roughness factor varies between 2 and 9, since the nano-structured features play a predominant role for such a variation.⁴⁶

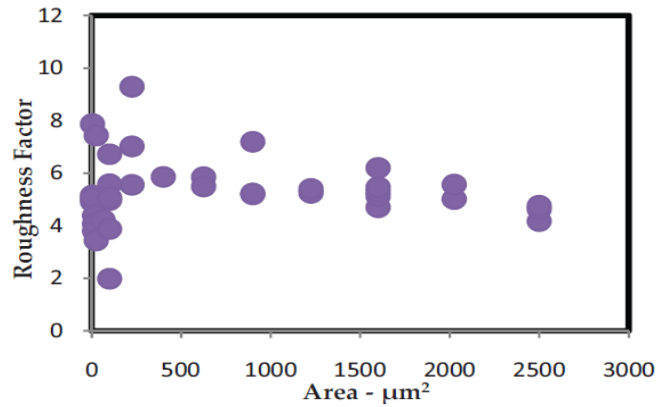


Fig.14: Variation of roughness factor with scan size

9. Cancer cell detection in tissue sections using afm

Presently, malignant growth analysis (cancer diagnosis) depends generally on morphological assessment of peeled, suctioned cells or precisely eliminated tissue. However long standard conclusion is concerned, this old style approach appears to be satisfactory. Breast, prostatic, and colorectal carcinomas have a place with the most regular malignant growth types these days. One of methods, delicate to changes in mechanical properties, is the Atomic force microscopy, which distinguishes cancer growth cells through their flexible properties. Such estimations were applied to tissue areas gathered from patients experiencing different tumours. This AFM technique was basically used to probe elasticity of tissues sections originating from various cancers showed distinct characteristics revealing the heterogeneity and complexity of tissue sections. However, despite the level of cancer tissue complexity, the use of the Young's modulus as an indicator of cancer alterations in a patient's sample was possible in the studied cancer cases, and gives hope to work out a new tool in effective and more accurate identification of cancer.

The heterogeneity of a cell structure plays a dominant role, usually leading to the broadening of the Young's modulus distribution (Fig. 2A and B). It is difficult to establish such an analysis based on only few measurements performed at one particular position on a cell surface. The strategy should

assume large number of measurements performed for a large number of cells at different locations over a single cell.

Once such dataset is obtained, the Young's modulus is determined from the Gaussian fit to the total histogram composed of all values determined for all cells which were found to be quite large. However, despite the large modulus distributions for normal cells, the Student's t-test showed significant differences between the means.

The Student's t-test showed significant differences between the means of normal and cancerous cells at the level of $p < 0.001$. These results showed that independently of the cell types, the normal cells were characterized by larger Young's modulus value (Fig. 3A). It indicates their lower ability to deform as compared to cells coming from later stages of cancer progression⁵⁴.

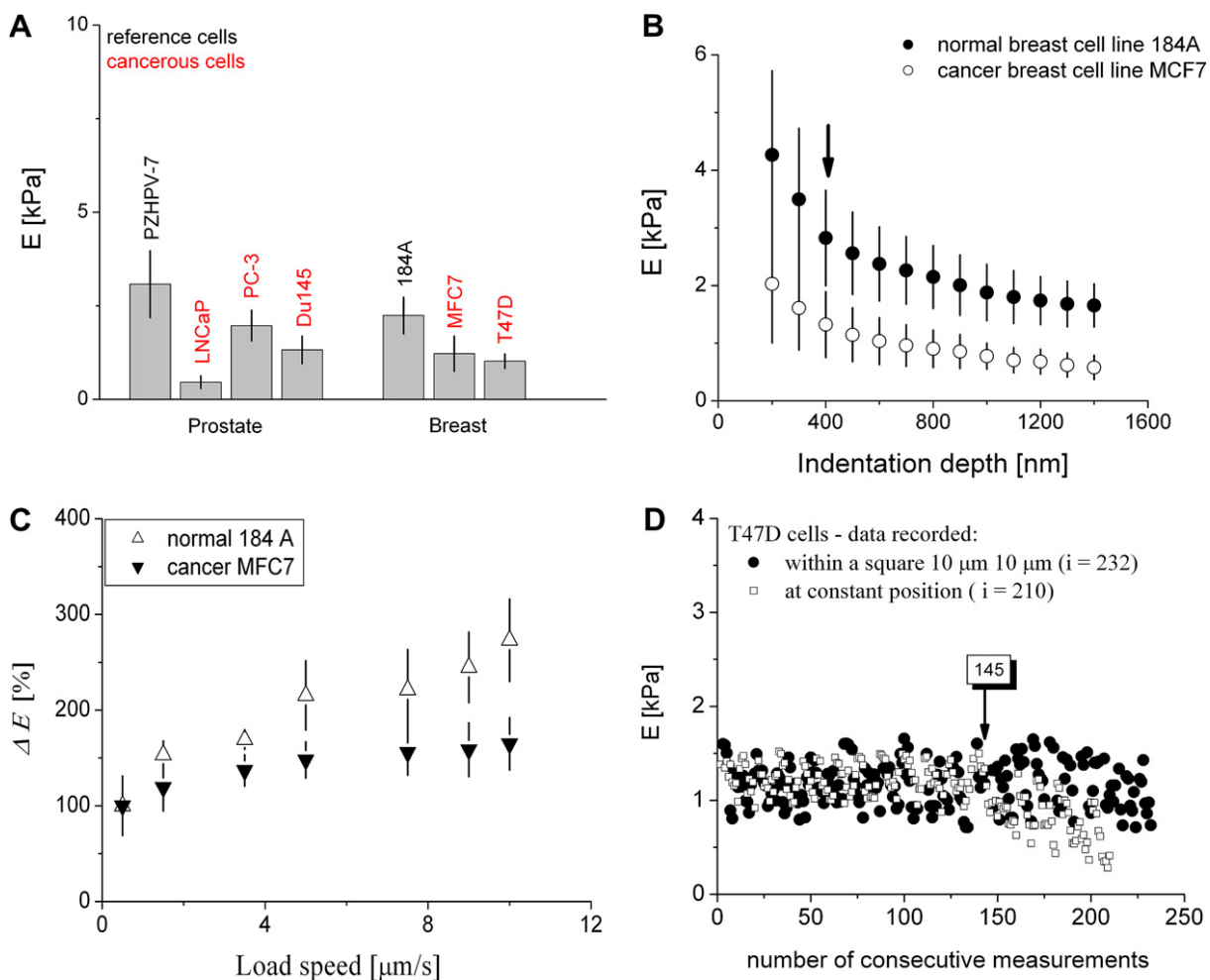


Fig.23: (A) Stiffness comparison for cells from prostate and breast cancers. Each column denotes the average Young's modulus (i.e. mean± standard deviation) determined for at least 30 cells and the same indentation depth of 400 nm. (B) Dependence on the indentation depth obtained for two human breast cells (184A and MCF7, respectively). (C) Scanner velocity applied during approach as observed for normal and cancer breast cells, presented as a percentage of a change of the Young's modulus, (D) Young's modulus presented as a function of a number of consecutive force curve recorded during the measurements (ordered as a function of time). Black dots shows measurements carried out within the square of about 10 μ m \times 10 μ m (232 curves) while open squares shows curves recorded at the constant position.

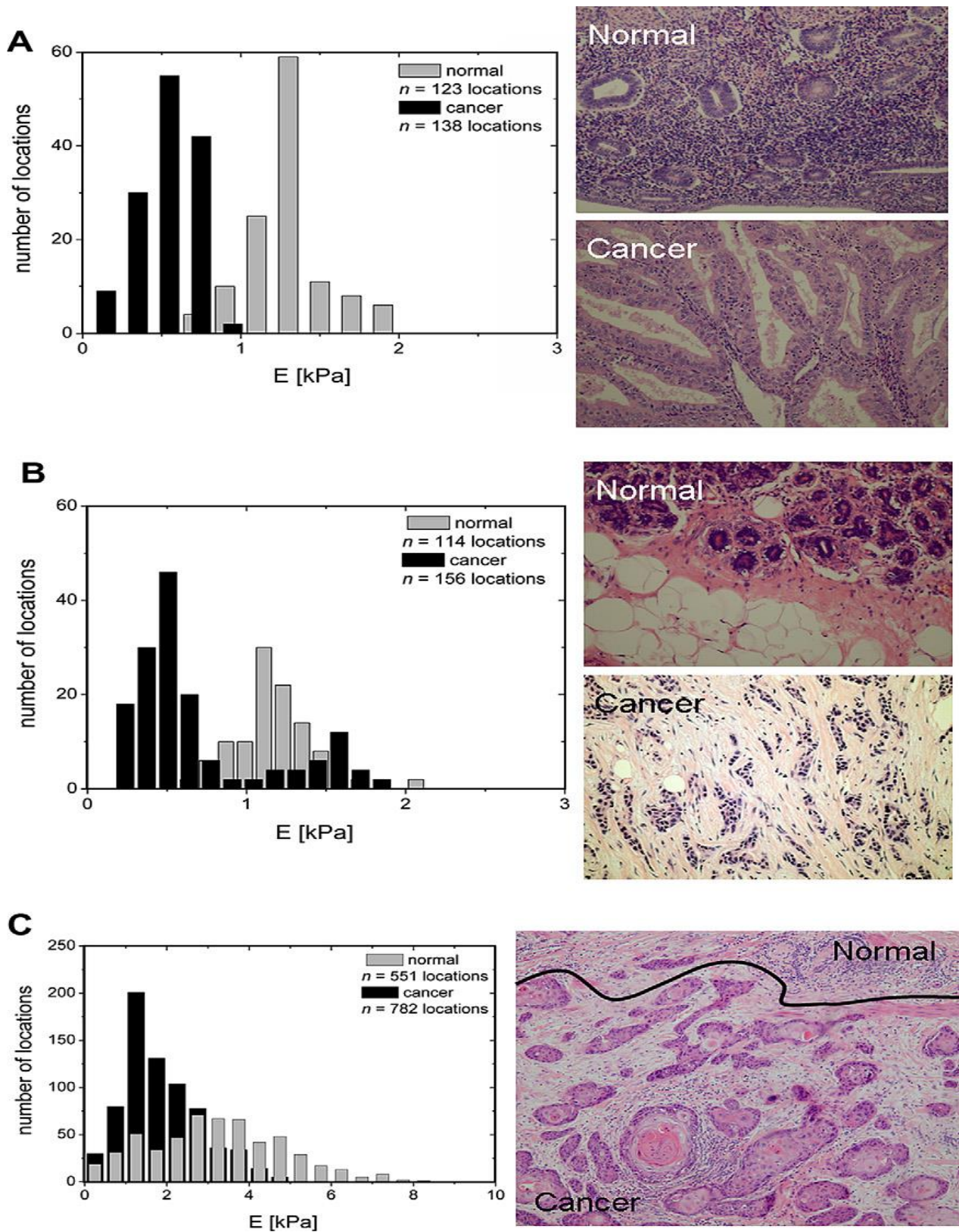


Fig.24: Stiffness distributions in tissues sections accompanied by the corresponding histological staining (hematoxylin–eosin, 400_x). (A) Nonneoplastic endometrium (gray columns) and well differentiated endometrioid carcinoma (black columns) of the uterine corpus. (B) Nonneoplastic breast tissue (gray columns) and infiltrating ductal carcinoma (black columns). (C) Vulvar cancer – black columns denote cancer while gray ones – nonneoplastic parts of the tissue section separated by black line in the histological image.

10. Study of galactomannose interaction with solids using afm, ir and allied techniques.

Guar gum (GG) and locust bean gum (LBG) are two galactomannose polysaccharides with different mannose/galactose ratio which is widely used in many industrial sectors including food, textiles, paper, adhesive, paint, pharmaceuticals, cosmetics and mineral processing. They are natural non-ionic polymers that are non-toxic and biodegradable. These properties make them ideal for industrial applications. However, a general lack of understanding of the interactions between the polysaccharides and solid surfaces has hindered wider application of these polymers. The atomic force microscopic (AFM) study was done with Nanoscope III (Digital instruments, Santa Barbara, CA). The measurements were performed underwater in tapping mode using a V-shaped Si₃N₄ cantilever covered with gold on the back for laser beam reflection. All images were collected in the height mode, which keep the force constant⁵⁵.

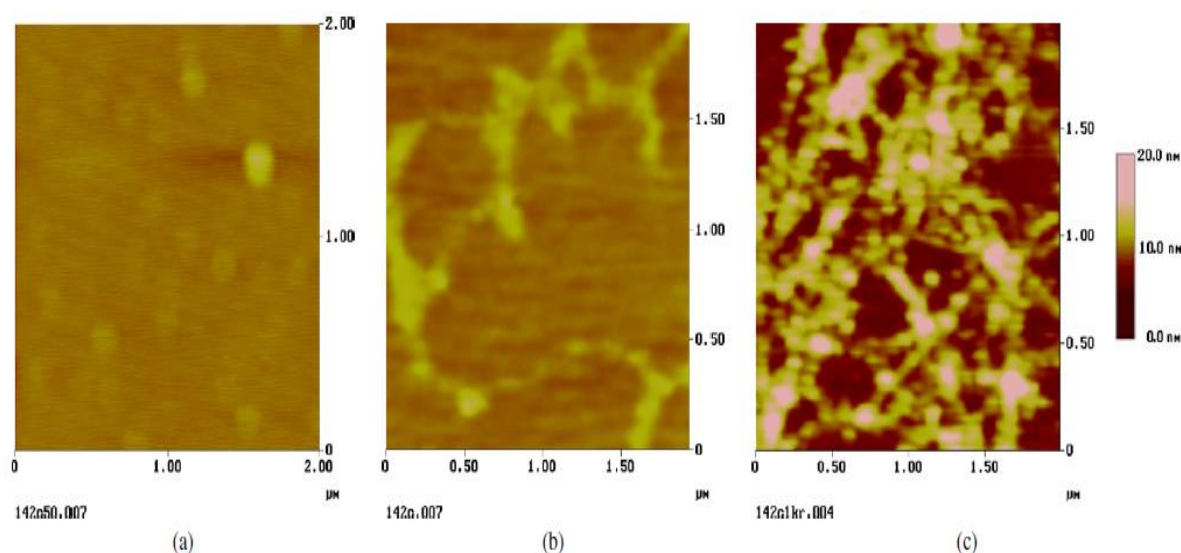


Fig.25: AFM images of guar gum adsorbed on mica at concentrations of (a)50ppm, (b)200ppm and (c) 1000ppm.

From AFM study^{56,57} of adsorbed guar gum at different concentration, it was found that guar gum first adsorb in the form of small clusters of about 1 nm thickness (Fig. 18a). Below maximum adsorption, the size of clusters increased with the increase in concentration (Fig. 18b), and further covered the surface fully with higher thickness (Fig. 18c), which suggest AFM was employed to further study the adsorbed topography of LBG and GG on solid. From Fig. 19, the surface coverage of these two different galactomannose on mica does not vary much. But LBG adsorbs in the form of isolated clusters with higher vertical distance. On the contrary, GG forms larger islands with lower thickness at the same concentration. From our computer simulation, it is apparent that LBG has more flexible structure than GG. In addition, since the galactose/ mannose ratio of LBG is lower than GG, the number of OH group on LBG that can form hydrogen bond with the solid surface is much less than that of GG, which explains why GG has a relatively flat conformation with lower thickness than LBG.

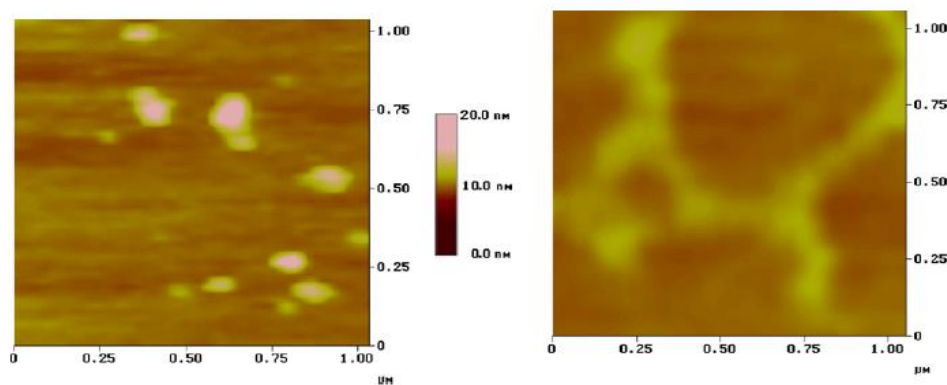


Fig.26: AFM images of gum with different M/G adsorbed on mica at (a) LBG, (b) GG(C:200ppm)

1. Atomic force microscopy in distinguishing nanoemulsions from nanocapsules

Nano - scaled drug delivery systems (NDDS) have become more and more important in improving drug therapy²⁴. AFM was performed to investigate the shape, morphology and mechanic properties of the emulsion and capsule shell. It proved to be a feasible technique to distinguish nanoemulsions from nanocapsules by stiffness analysis.

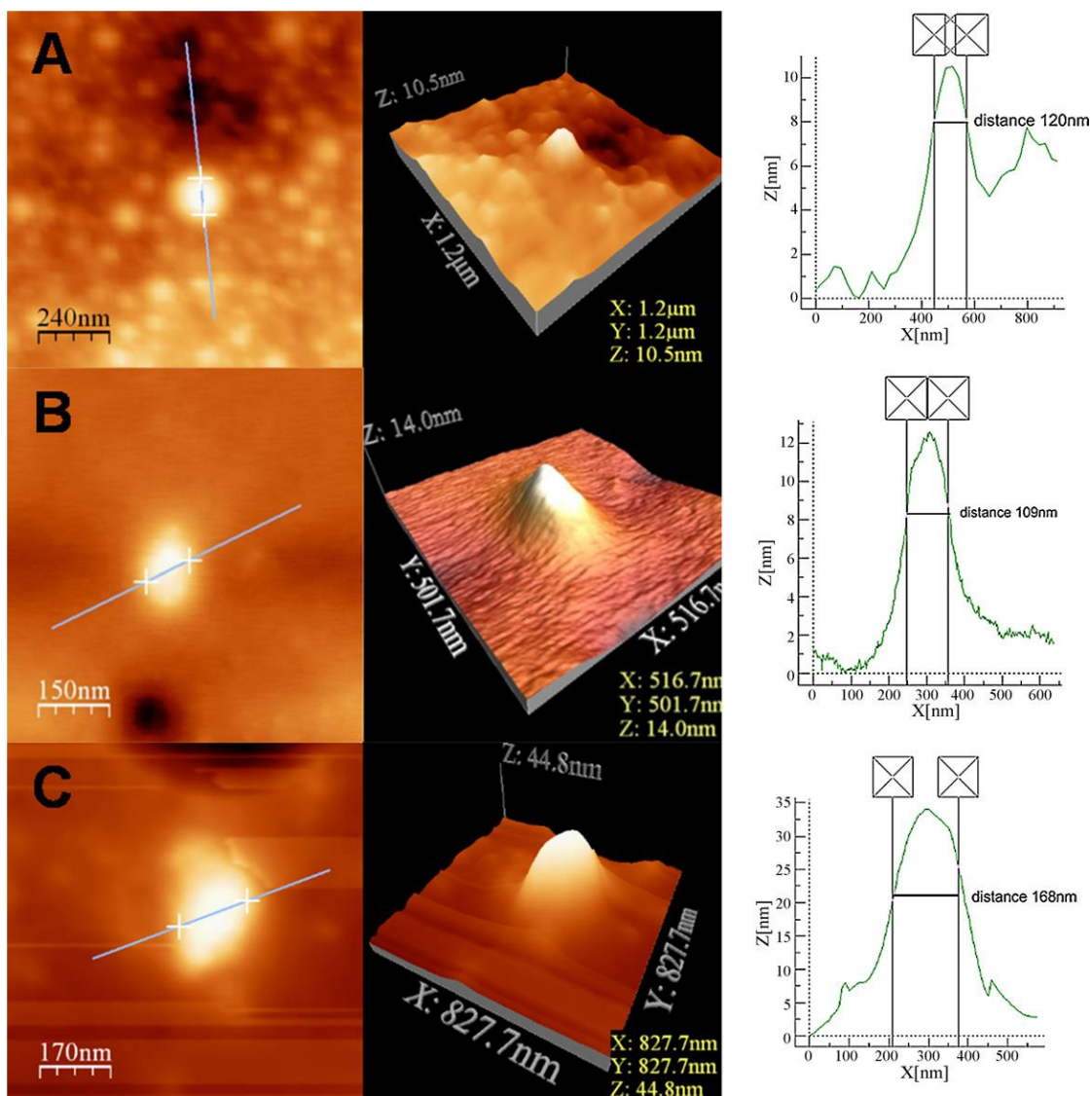


Fig.10: Topographic AFM images generated in tapping mode, left column: 2D-images, middle column: 3D-images, right column: height profiles; rows: (A) primary nanoemulsion, (B) three-layered nanocapsules, and (C) five-layered nanocapsules.

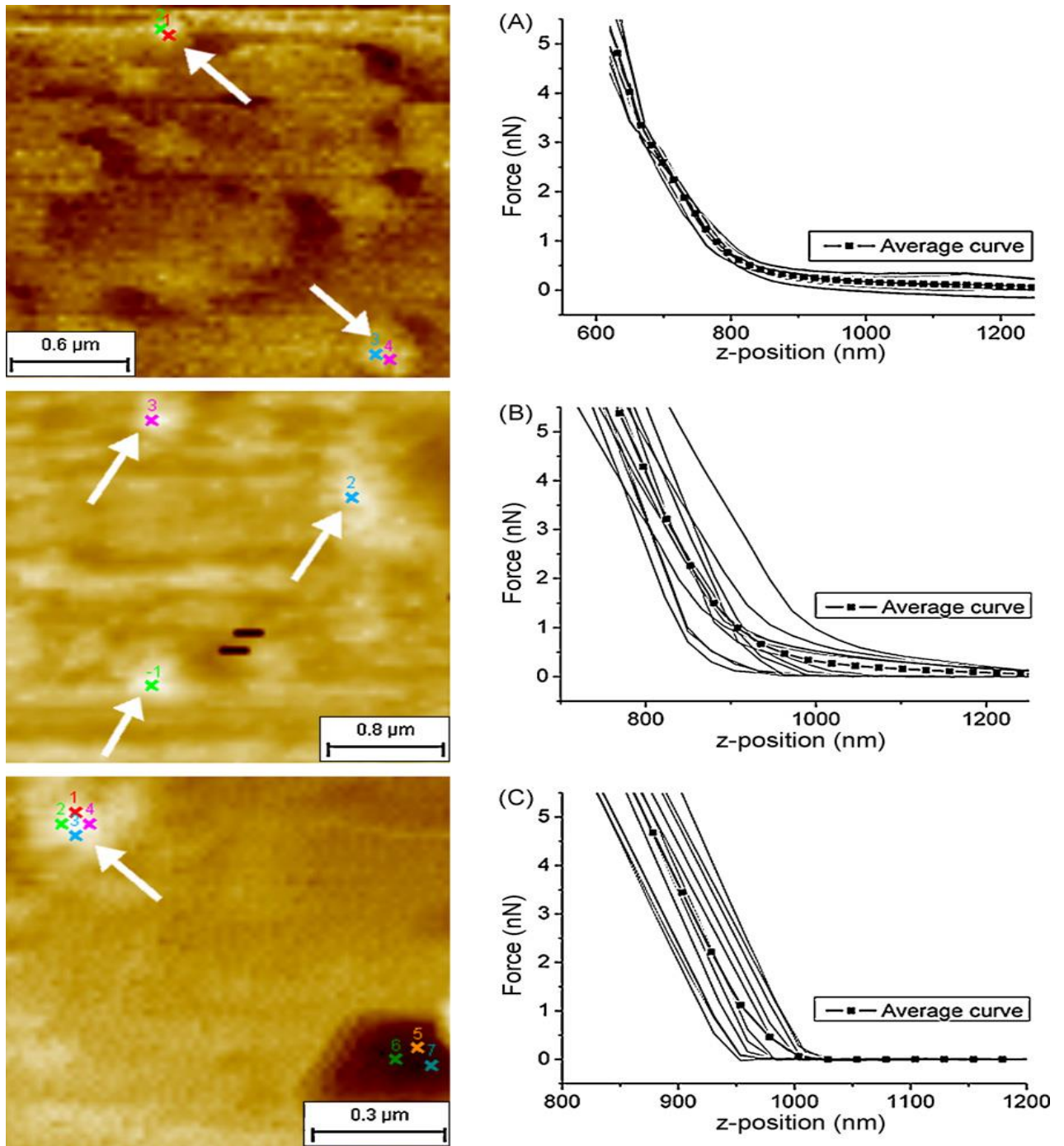


Fig.11: Left column: force–volume images generated in contact mode, arrows show positions of particles used for force curve analysis; Right column: 12 force–distance curves (approaching part) and average curve of each sample; (A) primary nanoemulsion, (B) three-layered nanocapsules, and (C) five-layered nanocapsules.

2. Afm as a nanotechnology tool in food science

AFM has been applied to investigate fine food molecule structure and molecular interaction on nanoscale. It has been successfully applied on qualitative and quantitative analysis of macromolecule structure, molecular interaction, and molecular manipulation. AFM has brought in much original knowledge on food properties and could be used to direct food processing and storage. By means of AFM, researchers have succeeded in modifying our previous understanding of the pectin molecular structures²⁹, proposed the degradation mode of pectin in fruits through the statistical results of pectin chain widths³⁰, and obtained direct process images of the molecular interactions between protein and surfactant. Unfortunately, not all the macromolecules have a good attachment to the mica surface. Therefore, it will be essential to modify the mica or the macromolecule in order to investigate or manipulate successfully.³¹

1. Afm in the study of Li deposition processes

It is well known that the performance of rechargeable Li batteries based on Li metal anodes depends on the morphology of the Li anodes upon charge-discharge cycling²⁷. When Li deposition in the electrolyte solution selected is not smooth but dendritic, the anode material is lost during cycling because the dendrites are disconnected from the bulk electrode by corrosion. Li particles of high surface area are formed, and consequently such a battery becomes dangerous upon heating, short, or exposure of the active materials to air. For this reason, a study of Li morphology upon cycling in the relevant electrolyte solutions for battery applications is important, and indeed, understanding the correlation between the morphology of the Li electrodes, the solution composition, and the geometry of the battery systems is essential for R&D of Li batteries. AFM to the study of Li electrodes (and probably other active metals) in aprotic systems. The basic electrochemical cell of the discoverer system (Topometrix) can be modified to hold the highly sensitive electrodes and solution and isolate them from atmospheric contaminants. The data obtained is meaningful, because scanning the tip over the electrode was found to be non-destructive and does not change the morphology on the surface, although Li metal is very soft. This may be partially attributed to the fact that the Li surfaces in solution are covered with surface species that are much harder than Li metal (e.g., Li salts). Although no struggle was faced to obtain very high resolution, the present studies obviously prove that the resolution obtainable by in situ AFM measurements is much higher than that obtained by SEM and may reach the 10 to 100 nm range and below²⁸.

2. Characterization of H-Benzo[cd]pyrene (OLYMPICENE) using AFM

H-Benzo[cd]pyrene ('Olympicene') is a polyaromatic hydrocarbon and non-Kekul fragment of graphene. A new synthetic method has been developed for the formation of 6H-benzo[cd]pyrene and related ketones including the first time isolation of the unstable alcohol 6H-benzo[cd]pyren-6-ol; AFM technique has been employed for its characterisation. To investigate the individual benzo[cd]pyrenes we deposited the molecules at a sample temperature of 10 K. Fig.15 shows constant-height AFM measurements of the observed species recorded with a CO tip.⁴⁷

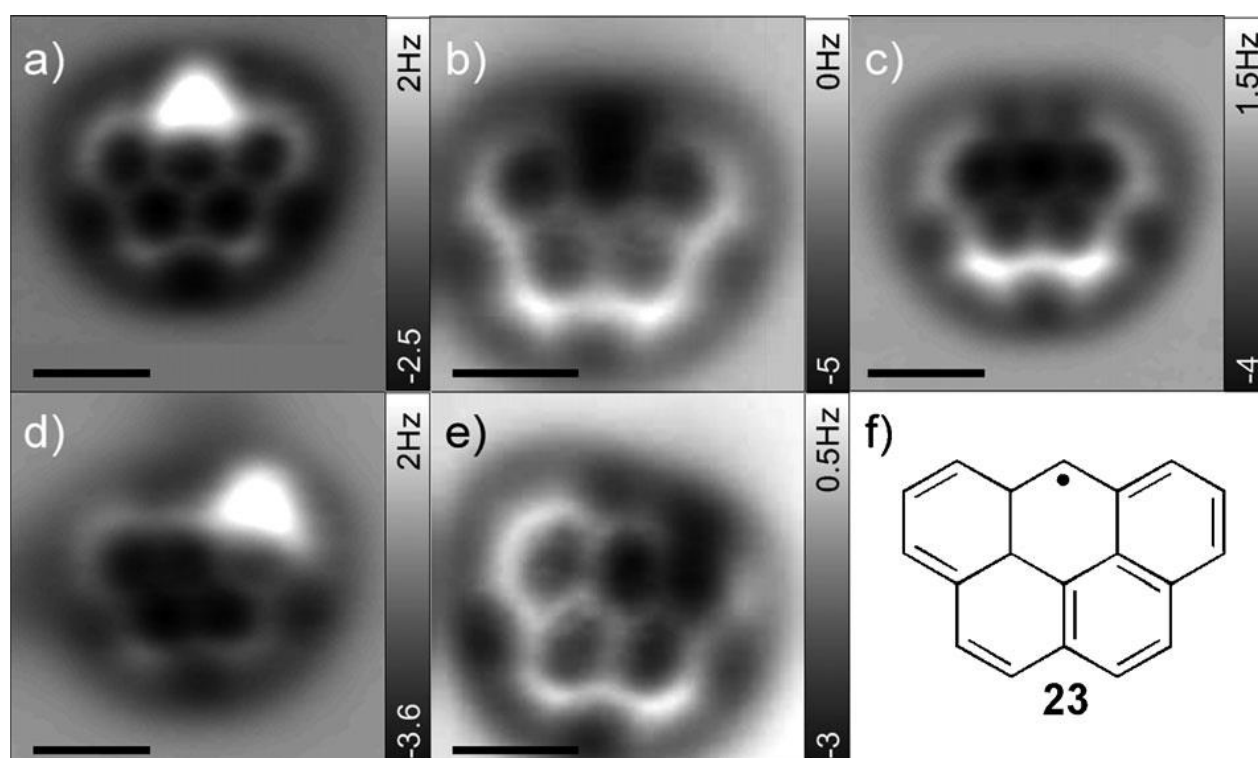


Fig.15: AFM images with CO tip functionalisation of a) 6H-benzo[cd]pyrene 8; b) 6-oxo-6H-benzo[cd]pyrene 7; c) benzo[cd]pyrene radical 23; d) 5H-benzo[cd]pyrene 6; e) 5-oxo-5H-benzo[cd]pyrene 5; in images a) and d) CH₂ groups can be seen as bright regions; in images b) and e) C=O can be seen as dark regions; f) The structure of benzo[cd]pyrene radical 23. The black scale bar equals 0.5 nm in all the images.

Some other organic compounds characterized under AFM are:

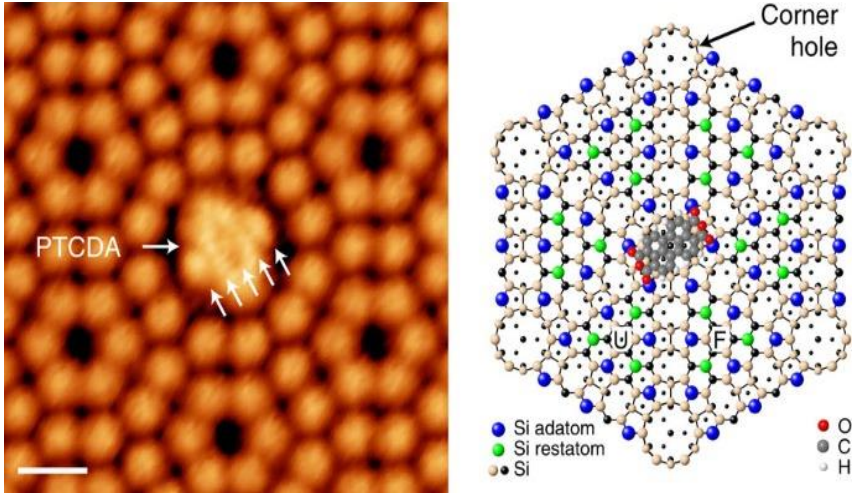


Fig.17: Perylene-3,4,9,10-tetracarboxylic dianhydride⁴⁸

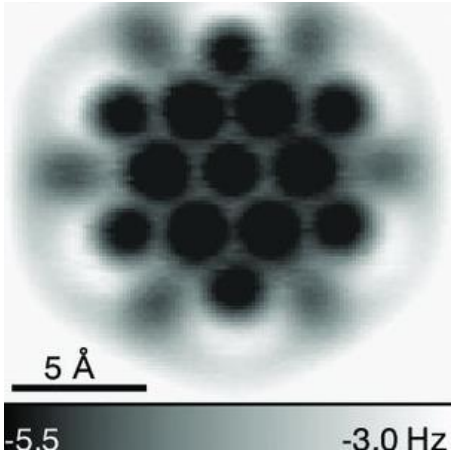


Fig.18: Hexabenzocoronene⁴⁹

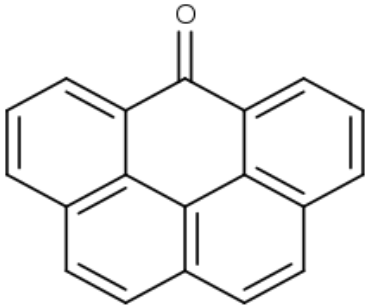


Fig.19: Napthanthrone⁵⁰

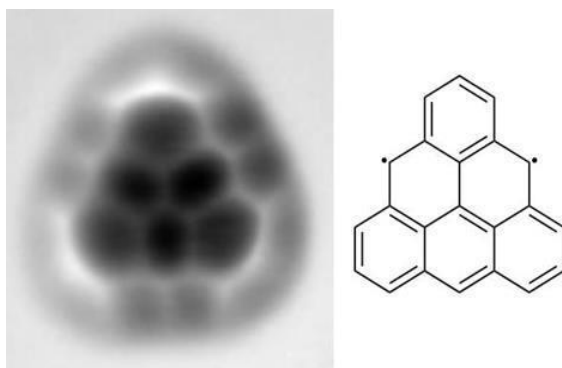


Fig.20: Triangulene⁵¹

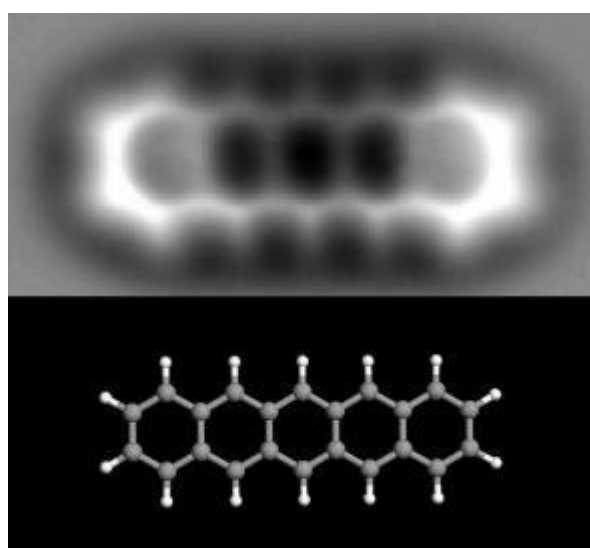


Fig.21: Pentacene⁵²

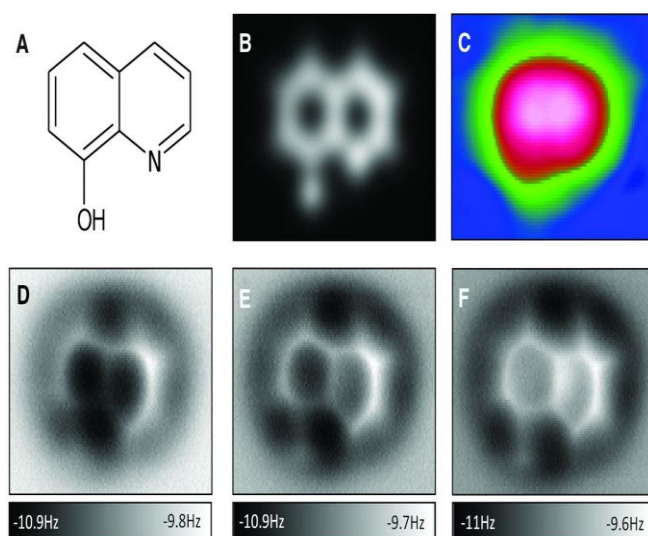


Fig.22: 8-hydroxyquinoline⁵³

3. Roughness and hydrophobicity of nanofiltration membranes using different modes of afm

Nanofiltration is one of the widely used techniques for the production of drinking water from surface water and ground water. But the major problem with this technique is fouling which arises due to the membrane technology which bears the suspended particulate matter¹⁸. This fouling is influenced by the parameters with respect to the solution itself i.e ionic strength and colloidal concentration; but the surface morphology plays an important role.

AFM non-contact mode and tapping mode were used to carry out the roughness measurements and it appeared that larger the scanned area larger the roughness. This phenomenon was related to the dependence of the roughness wavelength or frequency of the scanned area. All, the smaller as well as the larger frequencies or wavelengths are taken into consideration. This results in a larger roughness value. For smaller areas, the roughness of only the higher frequencies are measured.

A comparative study of these roughness values by changing the scan size was done with polymer assembled to nodules or aggregates of nodules which formed a fractal structure on the surface of the membrane. So, when the scan size is changed, it is possible to get a different topography resulting in different roughness value. Therefore, it should be noted that when comparing the surface roughness for different samples, same scan size must be maintained.

For Non-contact mode as well as tapping mode in AFM, a six membrane arrangement according to their surface roughness was used:

NTR7450 < NF-PES-10 < N30F < UTC-20 < Desal51HL < Desal 5DL, with NTR 7450 the smoothest membrane.

The roughness values are altogether different for the six nanofiltration layers, fluctuating from 8 to 52 Å in noncontact mode and from 5 to 68 Å in tapping mode for a checked area of $0.5 \times 0.5 \mu\text{m}^2$. This infers that the contrast between the smoothest film and the most roughest layer is the biggest in tapping mode AFM (63 Å versus 44 Å in non-contact mode). Fig.5 analyzes roughnesses got in noncontact AFM and in tapping mode AFM for an examined area of $0.5 \times 0.5 \mu\text{m}^2$ for the six nanofiltration films, along with the bisector of the diagram. The informative elements for the smoother films are situated under the bisector of the graph, implying that the roughness estimated in tapping mode is more quite smaller than in noncontact mode. The inverse is noticed for the more unpleasant films Desal 51HL and Desal 5DL. So tapping mode AFM brings about a bigger differentiation between the roughnesses of the layers. Comparative ends can be drawn for the other examined regions.

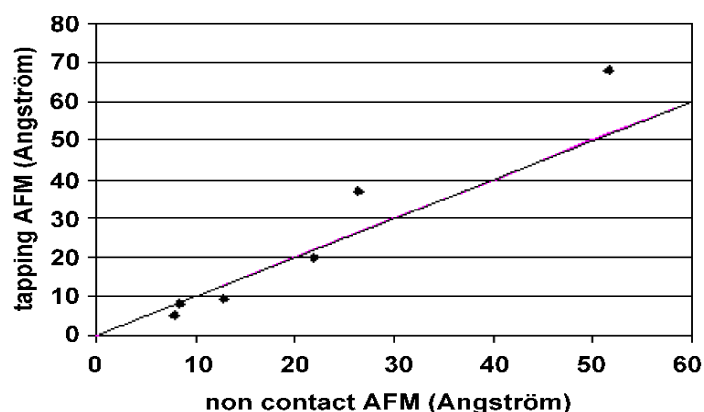


Fig. 5. Comparison between the roughness measured in noncontact AFM and the roughness measured in tapping mode AFM for an area of $0.5 \times 0.5 \mu\text{m}^2$.

This peculiarity is characteristic for the strategy for estimating harshness in tapping mode AFM. In tapping mode the tip (joined to the cantilever) taps the examined surface as opposed to noncontact AFM, where the distance between the tip and the surface is roughly 100 Å. Whenever a pollutant layer (e.g. a couple of monolayers of condensed water) covers the surface, an AFM working in tapping mode infiltrates the layer to picture the fundamental surface.

In noncontact mode, be that as it may, the AFM tip can't enter the water layer and subsequently it will picture the outer layer of the water layer. This outcomes in a more narrow distinction between the roughnesses of the different nanofiltration films in noncontact AFM. An additional advantage of tapping mode AFM is the simultaneous measurements of the phase shift, an essential alternative for the contact angle to study the hydrophobicity of the surface. The phase shift is extracted from the difference between the freely oscillating cantilever in air and the cantilever oscillation during scanning. If the tip does not interact with the sample then the phase shift is zero. However, a phase lag is induced if there is an attractive interaction between the tip and the sample. On the other hand, an advanced phase appears if the interaction is repulsive¹⁹.

4) Measurement and analysis of forces in bubble and droplet systems using afm.

In the mid-1990s, it was shown that, by connecting a colloidal molecule of a couple of microns width to the furthest limit of an AFM cantilever, the power between the molecule and a surface could be estimated⁵⁸. Utilizing this technique, exact data on electrical twofold layer and Van der Waals powers was acquired, with explicit pertinence to colloidal frameworks⁵⁸. Albeit the surface powers contraption (SFA)⁵⁹ had recently had the option

to give such understanding to explicit frameworks, the AFM offered a few reciprocal benefits with regards to the material mixes and geometries which could be investigated, done depending on crossed-chamber draws near between straightforward materials. A few years after the fact, the idea of expanding the estimation of colloidal powers utilizing the AFM to incorporate deformable bodies arisen.

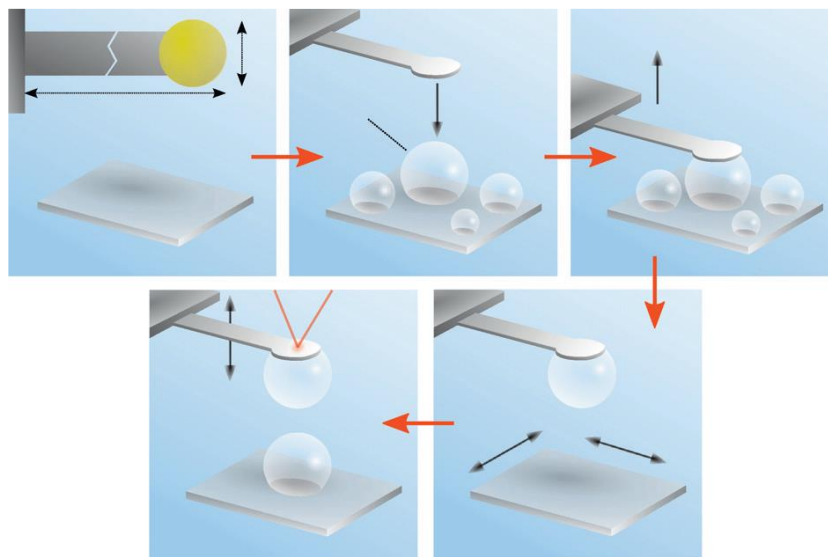


Fig.27: Schematic diagram showing how bubble or drop pair interactions are arranged in the AFM.

The underlying endeavors were estimations of balance powers between a strong molecule on the cantilever and an air pocket immobilized on a strong surface⁶⁰, and later between a molecule and oil bead⁶¹.

Bubbles and droplets provide many advantages over solid probes, not just for the case that one wishes to explore interactions between them. They can also be used as probes for the surface properties of other materials. In this capacity, they offer an unique and vital characteristic: when experiencing a repulsive force, a droplet or bubble will deform, increasing its effective area of interaction to many times greater than that of a hard sphere at close approach. This increased interaction area provides greater

sensitivity, and a more reliable and reproducible method for measuring such interactions. In addition, droplets and bubbles are exceptionally smooth, far smoother than the cleanest and least rough spheres, and hence can reliably achieve smaller separations and probe weaker forces than their rigid counterparts, provided the Laplace pressure permits. Droplets and bubbles also offer a wide range of options for controlling Van der Waals forces, to provide net repulsive or attractive interactions with solid surfaces, and to enhance or minimise the Van der Waals attraction between like pairs of droplets or bubbles in water. However, their inherent deformability raises challenges: when a solid particle is used as a probe, its position at all cantilever-surface separations can be known, by measuring the point of hard contact. As a droplet or bubble can deform in response to the forces it experiences, there is often no contact, and hence the separation is not clearly defined. Approaches to deduce the separation between deformable bodies and surfaces, and between pairs of droplets or bubbles rely on a combination of theoretical models and experimental measurements.

In addition, under certain circumstances, bubbles and droplets may coalesce when an attractive force dominates, and at sufficiently close approach. This property is unique to deformable systems, and is clearly of interest in systems where it is desirable to break an emulsion or foam to cause a bulk separation. However, it also means that post-coalescence, no more interactions can be measured between the two bodies, and hence another pair of droplets or bubbles must be found and scrutinised.

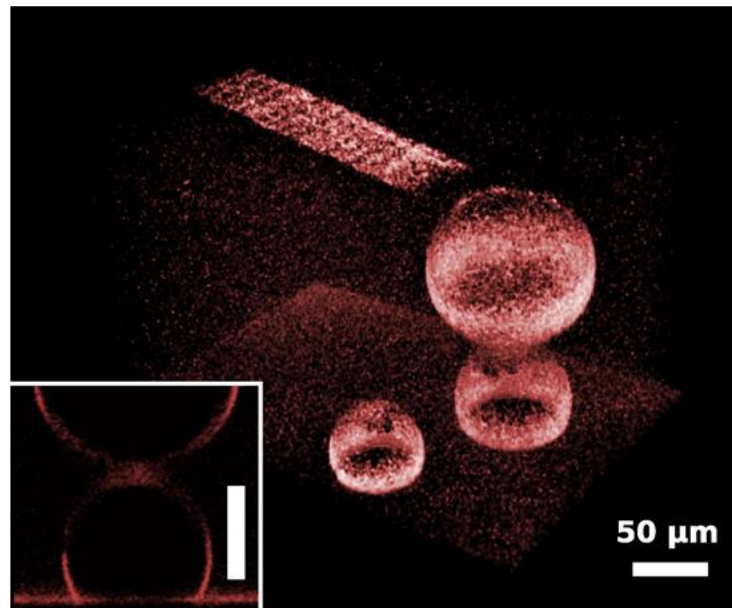


Fig.28: 3-Dimensional reconstruction obtained by laser scanning confocal microscopy, taken in situ in the AFM, just prior to a drop-drop interaction measurement. The inset shows a vertical ‘slice’ through the image, precisely half way through the two aligned drops.

A final issue is that drops and bubbles are by their nature dynamic entities. The curvature of their interfaces means that their internal Laplace pressure favours dissolution or Ostwald ripening, and hence their size may not be stable over the course of an AFM measurement, depending on its timescale. For fluorocarbon oils, whose water solubility is vanishingly low⁶², ripening is immeasurably slow, and hence of no concern for even the smallest drops. For hydrocarbon oils of C₁₀ and greater, their low aqueous solubilities also means that ripening is sufficiently slow to be of no concern in a typical AFM measurement.

Bubbles of moderately soluble gases (such as nitrogen, oxygen, argon) of around 100 μm will typically dissolve slowly enough to be considered stable over several minutes, allowing most AFM measurements to be completed with little concern. However, small bubbles (<30 μm), which have much higher internal Laplace pressures, dissolve much more quickly, and will change their size over a few tens of seconds.

When using highly soluble gases such as CO₂, ripening occurs in the bulk very rapidly, and is particularly problematic during the close approach of two bubbles, where for 100 l m bubbles, their radii will change significantly in a few seconds, making slow measurements impossible.

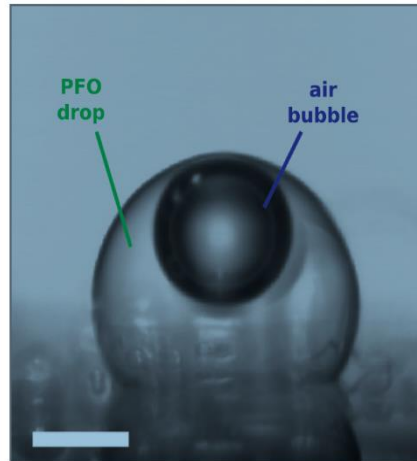


Fig.29: The end result of a hetero-coalescence event between a perfluorooctane (PFO) droplet that originated on the substrate and an air bubble that originated on the cantilever. The scale bar represents 100 l m.

A useful protocol is to measure the bubble radii microscopically before and after a measurement. If the agreement is poorer than a few l m, then the radii cannot be considered to be static throughout the measurement, and the data will be poorly defined. In any case, it was before long noticed that fundamentally more understanding could be acquired by getting an emulsion-scale bead onto the AFM cantilever⁶³. This permitted connections between sets of beads to be inspected, where somewhat high speeds could be utilized to investigate hydrodynamic waste impacts.

Major investigations have given a comprehension of when and how blend can happen in bubble frameworks ⁶⁴, the unforeseen charging properties of the uncovered oxidized gold surfaces utilized in practically all electronic gadgets, and the essential job of CO₂ in air bubble soundness⁶⁵, with expected ramifications for maritime spray.

ATOMIC FORCE MICROSCOPY FUTURE PROSPECTS

The Atomic force microscopy is an outstanding technique which incorporates the imaging of almost any type of sample ranging from biological samples to liquid samples. It does not require any sophisticated preparation of sample or metal or carbon coatings and the final image resolution remains intact. AFM can perfectly function in ambient air or even in a liquid environment. The improvements to AFM shall be aided by the scientists in the coming years which encompass the cantilevers and the merging power of AFM with other microscopic techniques. Scientists also predict that with these improvements in AFM will lead to understanding the rules of chemical reactions, a wide view of how to manipulate and create new molecules which were never reported before. Nuclear power microscopy (AFM) is in its thirties and has turned into a priceless apparatus for considering the miniature and nanoworlds. As an independent, high-goal imaging procedure and power transducer, it resists most other surface instrumentation in convenience, responsiveness and adaptability.

BIBLIOGRAPHY

1. Leggett, G. Atomic force microscopy. *Handb. Adhes. Second Ed.* 50–52 (2005) doi:10.1002/0470014229.ch1.
2. Mironov, V. L. Fundamentals of Scanning Probe Microscopy, The Textbook for Students of the Senior Courses of Higher Educational Institutions, The Russian Academy of Sciences. *Nizhniy Novgorod* (2004).
3. Engstfeld, A. K. Atomic scale STM imaging of alloy surfaces with chemical resolution. *Encycl. Interfacial Chem. Surf. Sci. Electrochem.* 39–47 (2018) doi:10.1016/B978-0-12-409547-2.12803-3.
4. Leung, C. & Palmer, R. E. Interfacing cluster physics with biology at the nanoscale. *Sci. Technol. At. Mol. Condens. Matter Biol. Syst.* **1**, 517–556 (2010).
5. Khan, I., Saeed, K. & Khan, I. Nanoparticles: Properties, applications and toxicities. *Arab. J. Chem.* **12**, 908–931 (2019).
6. Marrone, P. Chambers, RT. *Etica e Polit.* **15**, 583–605 (2013).
7. Leiro, J. A., Torhola, M. & Laajalehto, K. The AFM method in studies of muscovite mica and galena surfaces. *J. Phys. Chem. Solids* **100**, 40–44 (2017).
8. Gupta, V., Hampton, M. A., Nguyen, A. V. & Miller, J. D. Crystal lattice imaging of the silica and alumina faces of kaolinite using atomic force microscopy. *J. Colloid Interface Sci.* **352**, 75–80 (2010).
9. Siretanu, I., Van Den Ende, D. & Mugele, F. Atomic structure and surface defects at mineral-water interfaces probed by: In situ atomic force microscopy. *Nanoscale* **8**, 8220–8227 (2016).
10. Hampton, M. A., Plackowski, C. & Nguyen, A. V. Physical and chemical analysis of elemental sulfur formation during galena surface oxidation. *Langmuir* **27**, 4190–4201 (2011).
11. Xie, L. *et al.* Probing surface interactions of electrochemically active galena mineral surface using atomic force microscopy. *J. Phys. Chem. C* **120**, 22433–22442 (2016).
12. Bruening, F. A. & Cohen, A. D. Measuring surface properties and oxidation of coal macerals using the atomic force microscope. *Int. J. Coal Geol.* **63**, 195–204 (2005).

13. Fotiadis, D., Scheuring, S., Müller, S. A., Engel, A. & Müller, D. J. Imaging and manipulation of biological structures with the AFM. *Micron* **33**, 385–397 (2002).
14. Jaschke, M. *et al.* The atomic force microscope as a tool to study and manipulate local surface properties. *Biosens. Bioelectron.* **11**, 601–612 (1996).
15. Thalhammer, S., Stark, R. W., Müller, S., Wienberg, J. & Heckl, W. M. The atomic force microscope as a new microdissecting tool for the generation of genetic probes. *J. Struct. Biol.* **119**, 232–237 (1997).
16. Alonso, J. L. & Goldmann, W. H. Feeling the forces: Atomic force microscopy in cell biology. *Life Sci.* **72**, 2553–2560 (2003).
17. Geisler, B., Noll, F. & Hampp, N. Nanodissection and noncontact imaging of plasmid DNA with an atomic force microscope. *Scanning* **22**, 7–11 (2000).
18. Nghiem, L. D., Schäfer, A. I. & Waite, T. D. Adsorptive interactions between membranes and trace contaminants. *Desalination* **147**, 269–274 (2002).
19. Boussu, K. *et al.* Roughness and hydrophobicity studies of nanofiltration membranes using different modes of AFM. *J. Colloid Interface Sci.* **286**, 632–638 (2005).
20. de Beer, D., Stoodley, P., Roe, F. & Lewandowski, Z. Effects of biofilm structures on oxygen distribution and mass transport. *Biotechnol. Bioeng.* **43**, 1131–1138 (1994).
21. Bremer, P. J., Geese, G. G. & Drake, B. Atomic force microscopy examination of the topography of a hydrated bacterial biofilm on a copper surface. *Curr. Microbiol.* **24**, 223–230 (1992).
22. Beech, I. B., Cheung, C. W. S., Johnson, D. B. & Smith, J. R. Comparative studies of bacterial biofilms on steel surfaces using atomic force microscopy and environmental scanning electron microscopy. *Biofouling* **10**, 65–77 (1996).
23. Ushiki, T., Hitomi, J., Ogura, S., Umemoto, T. & Shigeno, M. Atomic force microscopy in histology and cytology. *Arch. Histol. Cytol.* **59**, 421–431 (1996).
24. Preetz, C., Hauser, A., Hause, G., Kramer, A. & Mäder, K. Application of atomic force microscopy and ultrasonic resonator technology on nanoscale: Distinction of nanoemulsions from nanocapsules. *Eur. J. Pharm. Sci.* **39**, 141–151 (2010).

25. Cheng, S., Bryant, R., Doerr, S. H., Rhodri Williams, P. & Wright, C. J. Application of atomic force microscopy to the study of natural and model soil particles. *J. Microsc.* **231**, 384–394 (2008).
26. Rabinovich, Y. I., Adler, J. J., Ata, A., Singh, R. K. & Moudgil, B. M. Adhesion between nanoscale rough surfaces. I. Role of asperity geometry. *J. Colloid Interface Sci.* **232**, 10–16 (2000).
27. Aurbach, D., Markovsky, B., Shechter, A., Ein-Eli, Y. & Cohen, H. A Comparative Study of Synthetic Graphite and Li Electrodes in Electrolyte Solutions Based on Ethylene Carbonate-Dimethyl Carbonate Mixtures. *J. Electrochem. Soc.* **143**, 3809–3820 (1996).
28. Aurbach, D. & Cohen, Y. The Application of Atomic Force Microscopy for the Study of Li Deposition Processes. *J. Electrochem. Soc.* **143**, 3525–3532 (1996).
29. Round, A. N., Rigby, N. M., MacDougall, A. J., Ring, S. G. & Morris, V. J. Investigating the nature of branching in pectin by atomic force microscopy and carbohydrate analysis. *Carbohydr. Res.* **331**, 337–342 (2001).
30. Yang, H., An, H., Feng, G., Li, Y. & Lai, S. Atomic force microscopy of the water-soluble pectin of peaches during storage. *Eur. Food Res. Technol.* **220**, 587–591 (2005).
31. Yang, H. *et al.* Application of atomic force microscopy as a nanotechnology tool in food science. *J. Food Sci.* **72**, 65–75 (2007).
32. Higham, T. E., Russell, A. P., Niewiarowski, P. H., Wright, A. & Speck, T. The Ecomechanics of Gecko Adhesion: Natural Surface Topography, Evolution, and Biomimetics. *Integr. Comp. Biol.* **59**, 148–167 (2019).
33. Russell, A. P. & Higham, T. E. A new angle on clinging in geckos: Incline, not substrate, triggers the deployment of the adhesive system. *Proc. R. Soc. B Biol. Sci.* **276**, 3705–3709 (2009).
34. Tolpekina, T. V. & Persson, B. N. J. Adhesion and friction for three tire tread compounds. *Lubricants* **7**, 1–25 (2019).
35. Higham, T. E., Gamble, T. & Russell, A. P. On the origin of frictional adhesion in geckos: Small morphological changes lead to a major biomechanical transition in the genus *Gonatodes*. *Biol. J. Linn. Soc.* **120**, 503–517 (2017).

36. Russell, A. P., Baskerville, J., Gamble, T. & Higham, T. E. The evolution of digit form in Gonatodes (Gekkota: Sphaerodactylidae) and its bearing on the transition from frictional to adhesive contact in gekkotans. *J. Morphol.* **276**, 1311–1332 (2015).
37. Persaud, D., Werner, N. & Werner, Y. L. Foraging behaviour of three sphaerodactylin geckos on Trinidad and Tobago (Sauria: Gekkonomorpha: Sphaerodactylini: Gonatodes). *J. Nat. Hist.* **37**, 1765–1777 (2003).
38. J. Harmon, L., L. Harmon, L. & G. Jones, C. Competition and community structure in diurnal arboreal geckos (genus *Phelsuma*) in the Indian Ocean. *Oikos* **116**, 1863–1878 (2007).
39. Noble, T., Bunbury, N., Kaiser-Bunbury, C. N. & Bell, D. J. Ecology and co-existence of two endemic day gecko (*Phelsuma*) species in Seychelles native palm forest. *J. Zool.* **283**, 73–80 (2011).
40. Avila-Pires, T. C. S. *Lizards of Brazilian Amazonia (Reptilia: Squamata)*. *Zoologische Verhandelingen* vol. 299 (1995).
41. Olesen, J. M. & Valido, A. Lizards as pollinators and seed dispersers: An island phenomenon. *Trends Ecol. Evol.* **18**, 177–181 (2003).
42. Hansen, D. M., Kiesbüy, H. C., Jones, C. G. & Müller, C. B. Positive indirect interactions between neighboring plant species via a lizard pollinator. *Am. Nat.* **169**, 534–542 (2007).
43. Bègue, J. F., Sanchez, M., Micheneau, C. & Fournel, J. New record of day geckos feeding on orchid nectar in Reunion Island: Can lizards pollinate orchid species? *Herpetol. Notes* **7**, 689–692 (2014).
44. Wu, L. yan, Han, Z. wu, Qiu, Z. mei, Guan, H. ying & Ren, L. quan. The Microstructures of Butterfly Wing Scales in Northeast of China. *J. Bionic Eng.* **4**, 47–52 (2007).
45. Chen, G., Cong, Q., Feng, Y. & Ren, L. Study on the wettability and self-cleaning of butterfly wing surfaces. *Inst. Phys. Conf. Ser.* **180**, 245–251 (2003).
46. Wanasekara, N. D. & Chalivendra, V. B. Surface characterization of butterfly wings. *Proc. 2010 IEEE 36th Annu. Northeast Bioeng. Conf. NEBEC 2010* **02747**, 1–2 (2010).

47. Mistry, A. *et al.* The synthesis and STM/AFM imaging of 'Olympicene' benzo[cd]pyrenes. *Chem. - A Eur. J.* **21**, 2011–2018 (2015).
48. Rönfeldt, P., Reinsch, H., Poschmann, M. P. M., Terraschke, H. & Stock, N. Scandium Metal-Organic Frameworks Containing Tetracarboxylate Linker Molecules: Synthesis, Structural Relationships, and Properties. *Cryst. Growth Des.* **20**, 4686–4694 (2020).
49. Qin, J. S. *et al.* Creating Well-Defined Hexabenzocoronene in Zirconium Metal-Organic Framework by Postsynthetic Annulation. *J. Am. Chem. Soc.* **141**, 2054–2060 (2019).
50. Fujisawa, S., Oonishi, I., Aoki, J. & Iwashima, S. The Crystal and Molecular Structure of Naphthanthrone. *Bulletin of the Chemical Society of Japan* vol. 49 3454–3456 (1976).
51. Krebs, F. C. Synthesis, structure, and properties of azatriangulenium salts. *Chem. - A Eur. J.* **7**, 1773–1783 (2001).
52. Doerr, A. Keep your eye on the atom. *Nat. Methods* **6**, 792 (2009).
53. Zhang, J. *et al.* Real-space identification of intermolecular bonding with atomic force microscopy. *Science (80-.)*. **342**, 611–614 (2013).
54. Lekka, M. *et al.* Cancer cell detection in tissue sections using AFM. *Arch. Biochem. Biophys.* **518**, 151–156 (2012).
55. Wang, J. & Somasundaran, P. Study of galactomannose interaction with solids using AFM, IR and allied techniques. *J. Colloid Interface Sci.* **309**, 373–383 (2007).
56. McIntire, T. M. & Brant, D. A. Observations of the (1→3)- β -D-glucan linear triple helix to macrocycle interconversion using noncontact atomic force microscopy. *J. Am. Chem. Soc.* **120**, 6909–6919 (1998).
57. Chalykh, A. E., Matveev, V. V., Muravlev, D. A., Mityuk, D. Y. & Philippova, O. E. Nanostructure of xanthan networks. *Nanotechnologies Russ.* **12**, 1–8 (2017).
58. Ducker, W. A., Senden, T. J. & Pashley, R. M. Measurement of Forces in Liquids Using a Force Microscope. *Langmuir* **8**, 1831–1836 (1992).

59. Israelachvili, J. N. Adhesion forces between surfaces in liquids and condensable vapours. *Surf. Sci. Rep.* **14**, 109–159 (1992).
60. Claesson, P. M., Ederth, T., Bergeron, V. & Rutland, M. W. Techniques for measuring surface forces. *Adv. Colloid Interface Sci.* **67**, 119–183 (1996).
61. Chen, L., Heim, L. O., Golovko, D. S. & Bonaccorso, E. Snap-in dynamics of single particles to water drops. *Appl. Phys. Lett.* **101**, (2012).
62. Tabor, R. F., Gold, S. & Eastoe, J. Electron density matching as a guide to surfactant design. *Langmuir* **22**, 963–968 (2006).
63. Dagastine, R. R. *et al.* Dynamic forces between two deformable oil droplets in water. *Science (80-.)*. **313**, 210–213 (2006).
64. Vakarelski, I. U. *et al.* Dynamic interactions between microbubbles in water. *Proc. Natl. Acad. Sci. U. S. A.* **107**, 11177–11182 (2010).
65. Tabor, R. F., Morfa, A. J., Grieser, F., Chan, D. Y. C. & Dagastine, R. R. Effect of gold oxide in measurements of colloidal force. *Langmuir* **27**, 6026–6030 (2011).